scientific reports

Check for updates

OPEN

Predicting workability and mechanical properties of bentonite plastic concrete using hybrid ensemble learning

Amir Tavana Amlashi[1]✉, Ali Reza Ghanizadeh[2], Shadi Firouzranjbar[1], Hossein Moradi Moghaddam[3], Mohsen Navazani[1], Haytham F. Isleem[4,5]✉, Samer Dessouky[1] & Mohammad Khishe[6,7,8,9]✉

Heavy metal contamination in wastewater poses severe environmental challenges, highlighting the urgent need for efficient and cost-effective solutions. While bentonite incorporation in concrete mixtures has shown promise in adsorbing heavy metals, its experimental validation—through Bentonite Plastic Concrete (BPC)—is hindered by high costs, labor-intensive procedures, and the need for specialized equipment. This study overcomes these barriers by introducing hybrid ensemble learning models, optimized with Forensic-Based Investigation Optimization (FBIO), to predict BPC's workability and mechanical properties, including slump (S), tensile strength (TS), and elastic modulus (E). Using input parameters such as gravel, bentonite, silty clay, curing time, sand, cement, and water, models including Random Forest (RF), Adaptive Boosting (ADB), Extreme Gradient Boosting (XGB), and Gradient Boosting Regression Tree (GBRT) were developed. Notably, GBRT-FBIO achieved the highest accuracy for E predictions, while XGB-FBIO excelled for TS and S. Shapley Additive Explanation (SHAP) analysis identified water as the most critical factor influencing slump (+ 0.11) predictions while curing time emerged as the key determinant for TS (+ 0.18) and E (+ 0.12) predictions. Additionally, a user-friendly online tool was developed to enable the real-time application of these models, reducing reliance on costly experimental methods. This work addresses key challenges in experimental BPC testing, offering a transformative computational approach for advancing civil engineering materials research.

Keywords Bentonite plastic concrete, Ensemble learning, Forensic-based investigation optimization, Online application

As a global concern, waste management is one of the key issues that need to be moved across the globe towards sustainability[1]. Heavy metal contamination is created in wastewater from various industrial operations, including mining and plating various metals. Heavy metals, including Cr, Hg, Cu, Pb, Cd, Zn, and Ni, are ecologically dangerous since they do not dissolve and can gather in organisms[2,3]. Adsorption is commonly regarded as an economical and efficient approach to treatment for wastewater and toxic pollutant removal[4]. Clay minerals have recently gained a lot of interest as adsorbents for several harmful chemicals and heavy metals[5]. Clay minerals as an adsorbent have various advantages over other materials, including fair, easy access, low price, non-toxic nature, significant specific surface area, and high efficiency in cationic exchange[6]. Bentonite is mostly made up of the mineral montmorillonite, calcite, feldspar, and quartz. Several scholars have examined the use of bentonite for heavy metal adsorption throughout the recent decade[7–11]. One approach to removing

[1]School of Civil and Environmental Engineering and Construction Management, University of Texas at San Antonio, San Antonio, USA. [2]Department of Civil Engineering, Sirjan University of Technology, Sirjan, Iran. [3]School of Engineering, University of British Columbia, Kelowna, Canada. [4]Jadara University Research Center, Jadara University, Irbid, Jordan. [5]Department of computer Science, University of York, York YO10 5DD, UK. [6]Department of Electrical Engineering, Imam Khomeini Naval Science University of Nowshahr, Nowshahr, Iran. [7]Applied science research center, Applied Science Private University, Amman, Jordan. [8] Centre for Research Impact & Outcome, Chitkara University Institute of Engineering and Technology, Chitkara University, Rajpura, 140401, Punjab, India. [9] Department of Electronics and Communication Engineering, Graphic Era Hill University, Dehradun, India. ✉email: amir.tavanaamlashi@utsa.edu; mps565@york.ac.uk; m_khishe@alumni.iust.ac.ir

heavy metals is to include bentonite in materials like concrete mixtures. Bentonite plastic concrete (BPC) blends bentonite and typical concrete[12]. When exposed to water, bentonite may absorb it and expand in size. As a result of the bentonite's water absorption potential, plastic concrete has a desirable low permeability level[13]. Abbaslou et al.[14] investigated BPC's capacity to remove dissolved cadmium components from water. Plastic concrete physical parameters were improved and modified, resulting in fewer cracks and a longer working life for various engineering constructions. Despite these advantages, the effective prediction of BPC's mechanical properties, including slump, tensile strength, and elastic modulus, remains challenging due to experimental methods' laborious and costly nature.

BPC is commonly used to build cut-off walls to decrease dam seepage. Dam water seepage reduces internal friction and causes the dam to slide or collapse[15]. BPC is gaining popularity due to its advantageous attributes, including its elastic-plastic features, low permeation, and uniformity[16]. Plastic concrete should tolerate strain between the wall and nearby soil to reduce the risk of excessive wall strain and facilitate displacement without separation. BPC should have great workability and homogeneity for easier filling of trenches and deep walls. However, the technical challenges of ensuring consistent mix design and predicting mechanical properties efficiently have limited its broader application. Addressing these gaps through computational methodologies is critical.

Previous studies on computational techniques for predicting BPC properties can be divided into three categories. The first group includes studies utilizing single machine learning (ML) models like artificial neural networks (ANN), M5 Tree, and Multivariate Adaptive Regression Splines (MARS)[17–19]. These models are more precise and robust than traditional regression methods in predicting green concrete characteristics[20]. ML techniques allow for accurate predictions of material properties, such as compressive strength and fracture toughness, without extensive experimentation[21–23]. Tavana Amlashi et al.[19] demonstrated that ANN outperforms M5 Tree and MARS in predicting BPC slump, elastic modulus, and compressive strength. Ghanizadeh et al.[24] employed SVM and ANN to forecast BPC compressive strength, identifying cement as the most influential factor. Tavana Amlashi et al.[25] combined SVM, ANN, and Adaptive Neuro-Fuzzy Inference System (ANFIS) with Particle Swarm Optimization (PSO) to predict compressive and splitting tensile strength, with ANN-PSO achieving an R^2 of 0.95, outperforming other methods. In another study, Tavana Amlashi et al.[26] used four computational techniques—Response Surface Methodology (RSM), Multigene Genetic Programming (MGGP), Group Method of Data Handling (GMDH), and SVM—to predict the compressive strength of BPC, based on parameters like water, silty clay, sand, gravel, cement, and bentonite.

The second group focuses on ensemble learning (EL) models, like Gradient Boosting Regression Trees (GBRT), Random Forests (RF), and Extreme Gradient Boosting (XGB). Alishvandi et al.[27] applied six computational methods—GBRT, Decision Tree (DT), RF, XGB, k-Nearest Neighbors (KNN), and SVM—for predicting the compressive strength of plastic concrete using factors like temperature, bentonite, cement, sand, water, and water-to-cement ratio. Model performance was evaluated using R^2, RMSE, MAE, and MAPE. EL methods outperform individual ML algorithms[28] in predicting the mechanical properties of various concrete types, including high-performance concrete (HPC)[29–35], recycled aggregate concrete (RAC)[36–39], lightweight foamed concrete (LFC)[40], geopolymer concrete (GPC)[41,42], self-compacting concrete (SCC)[43], and concrete with rice husk ash (CCRHA)[44–47]. EL methods are categorized into stacking, boosting, and bagging techniques. Boosting models such as Adaptive Boosting (ADB), GBRT, and XGB are widely used[29]. Li and Song[46] demonstrated that stacking EL models, with XGB as a base learner and linear regression as the second layer, enhances model precision by integrating base learners' outputs. ADB assigns weights to training samples based on regression difficulty, creating a meta-learning model suitable for simple and complex data[48]. GBRT, a boosting method employing an additive model and residual reduction, uses CART to fit negative gradients of loss functions during training[49,50]. Bagging methods, such as RF, have also shown superior performance. Amin et al.[45] reported that RF outperformed DT and ADB in compressive strength estimation of CCRHA. According to Iftikhar et al.[47], an improved RF model using EL increased compressive strength prediction accuracy by 1.62% compared to standalone RF models.

The third group of models incorporates optimization techniques like Particle Swarm Optimization (PSO) and forensic-based investigation optimization (FBIO) to fine-tune hyperparameters in boosting and bagging algorithms, thereby improving accuracy and efficiency. Tuning meta-parameters is critical for developing ensemble learning (EL) systems[51]. However, the abundance of meta-parameters complicates the process, requiring a thorough understanding of their impacts on model outcomes[52]. This task is time-intensive and computationally demanding. Researchers have introduced various methods to simplify the development of EL models, aiming to reduce manual effort while enhancing performance within limited timeframes[53–57]. This research utilizes the FBIO method to optimize global meta-parameters for boosting and bagging algorithms[48]. FBIO ensures optimal performance by automating parameter tuning, alleviating manual selection challenges, and expediting EL model improvement[58].

In this study, we address the challenges of predicting BPC's mechanical properties by employing a novel approach that combines ensemble learning with FBIO for hyperparameter optimization. Using large laboratory datasets, we develop robust models capable of accurately estimating slump, tensile strength, and elastic modulus. Furthermore, to overcome the black-box nature of machine learning methods, we design an online, user-friendly application to facilitate the implementation of the suggested model by engineers on-field. This study aims to bridge the gap between theoretical advancements in ML and practical applications in BPC design, providing engineers with reliable tools to improve project efficiency and sustainability.

Methodology

ADB

Schapire introduced the boosting method in 1990, which involves combining multiple weak learners in a series[59]. Equation 1 illustrates that the entire tree is replaced upon introducing a new tree model to the system, retaining only the strongest one. The iterative nature of computations leads to cumulative improvements in the overall model performance over time. The ADB approach continuously improves data categorization skills by training inside a suboptimal classification framework. This method assigns various weights to the input data to enhance classification accuracy[60]. This model focuses more on improving the classification of the incorrectly categorized samples[61]. Despite being a weak learner, ADB encompasses all machine learning regression techniques. Notably, DT regression and ANN are widely used within this framework. Decision Trees are preferred due to their extensive application across technical domains and the ease of model training. Various sources provide a comprehensive intellectual foundation for Decision Trees[62]. Figure 1 provides an overview of the ADB model. Training results differed because each training data set was unified, and the results were finally merged.

$$\mathrm{F_n(x)} = \mathrm{F_{n\,-\,1}(x)} + \mathrm{argmin}_h \sum_{\mathrm{i}=1}^{\mathrm{n}} \mathrm{L(y_i)},\ \mathrm{F_{n\,-\,1}(x_i)} + h(x_i) \tag{1}$$

In this context, the comprehensive model is denoted as *Fn(x)* , where "n" represents the current cycle, and the model from the preceding cycle is represented as *Fn-1(x)*. Furthermore, $h(x_i)$ refers to the recently added tree, and y_i signifies the anticipated result of the *i-th* tree.

GBRT

Breiman et al.[63] presented the CART method. CARTs could be applied to classification and regression methods[64–66]. Recursive techniques are employed to construct binary trees, which are the decision trees utilized in regression and classification methods. This study primarily focuses on the GBRT model developed by He et al.[67], which combines the Gradient Boosting and CART methods. The CART is acknowledged for its higher forecasting precision than other artificial intelligence methods. The CART method generates regression trees serving as weak learners, as the GBRT model transforms these weak learners into more effective ones. The algorithm incorporates poor learners to refine previously obtained predictions, aiming to reduce forecasting errors and enhance overall reliability.

The associated leaf node region of the *m*th regression tree in the updated algorithm, denoted as $F_m(x)$, or $R_{m,j}$, where $j = 1, 2, \ldots, J_m$, is determined by Eq. 2:

$$\mathrm{F_m(x)} = \mathrm{F_{m\,-\,1}(x)} + \sum_{j=1}^{J_m} \mathrm{c_{m,j}} \mathrm{I}(x \in \mathrm{R_{m,j}}) \tag{2}$$

I is around 1 if $x \in R_{m,j}$ and 0 otherwise[68]. The leaf node number in the *m*th regression tree is either denoted by J_m. The model is updated accordinglyFig. e 2 provides an overview of the GBRT model.

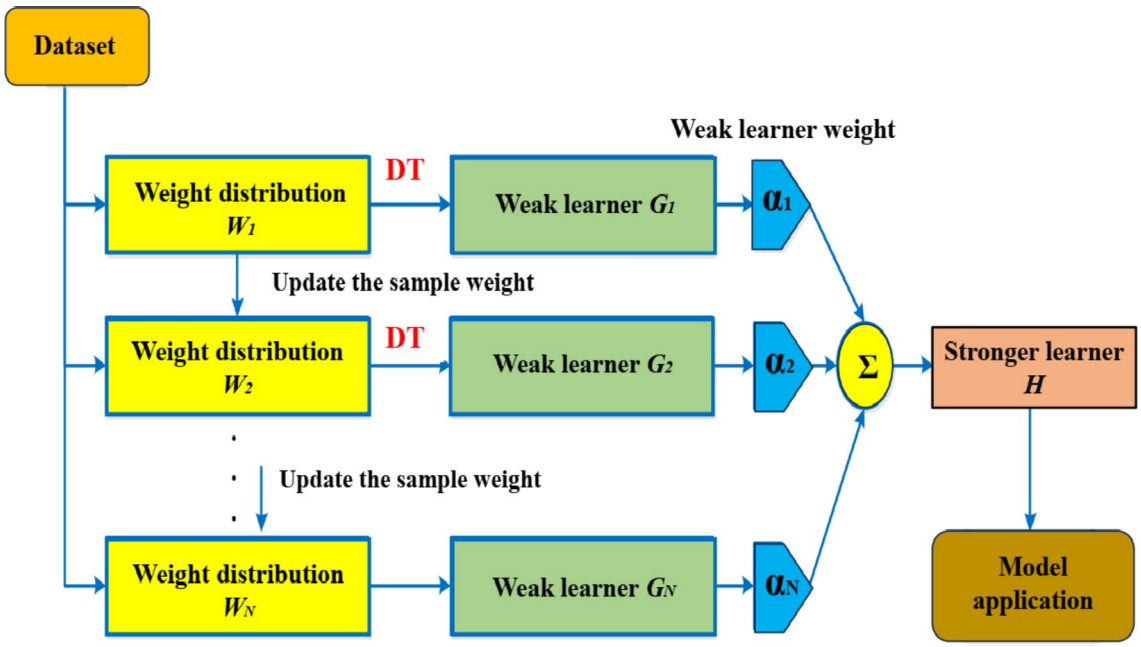

Fig. 1. The sequence of steps in the ADB modeling process.

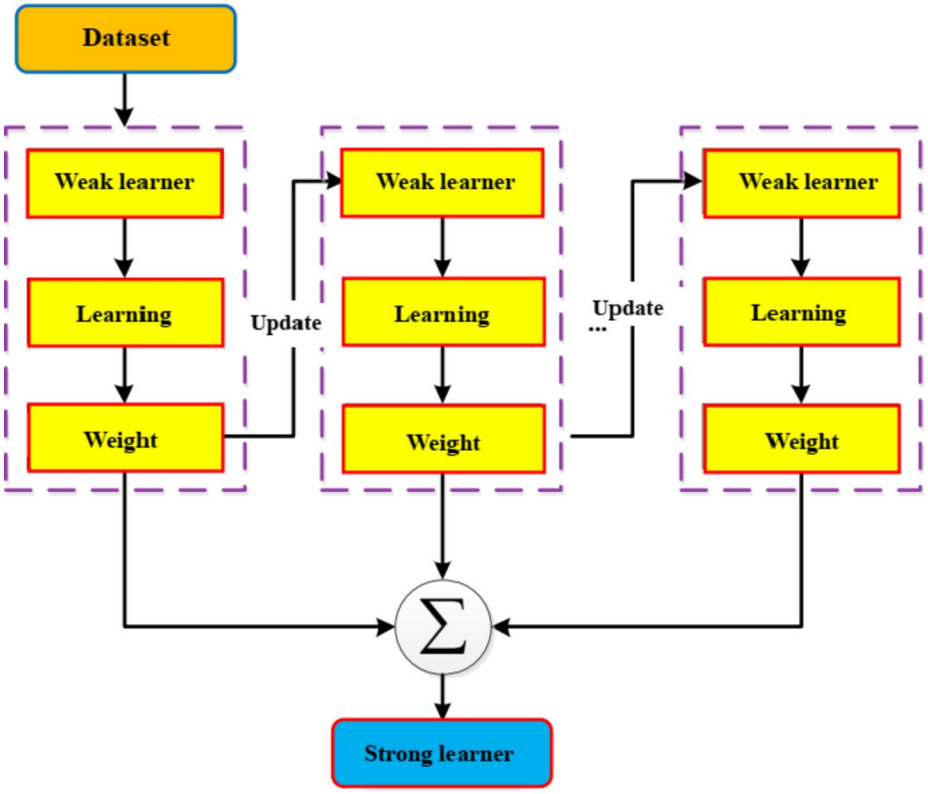

Fig. 2. The basic process of GBRT.

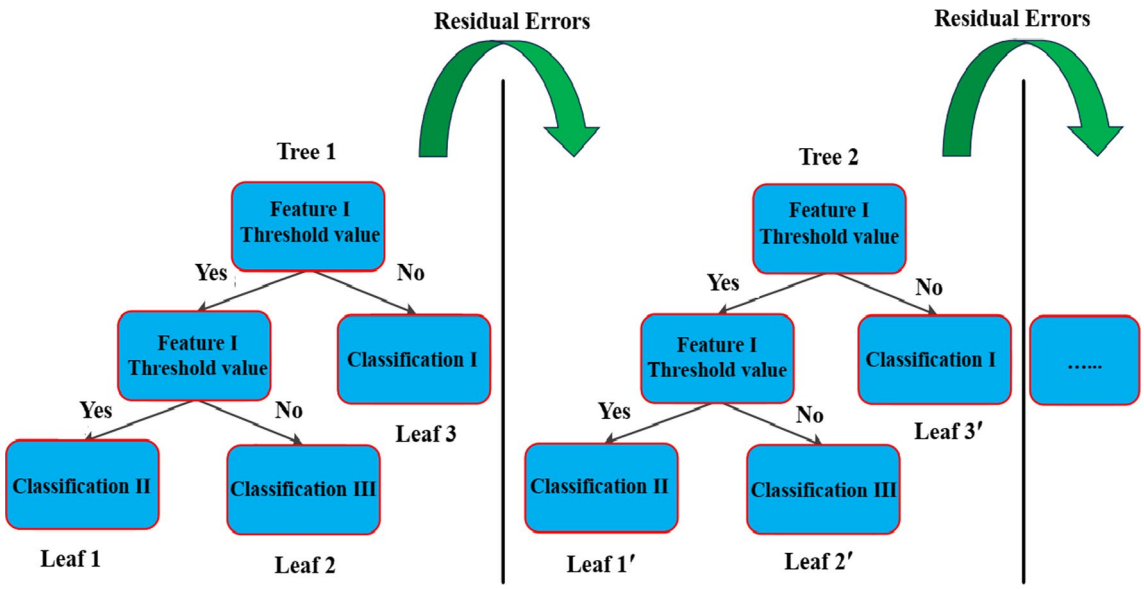

Fig. 3. A flowchart depicting the structure of XGB trees.

XGB

Chen and He[69] are credited with developing the XGB methodology. XGB effectively addresses both regression and classification tasks by constructing boosted trees. This serves as the foundation of the XGB algorithm and is analogous to various optimization models. XGB offers a dependable and quick simulation model like the GBRT decision tree. The XGB algorithm is defined by (Fig. 3).

The objective function of XGB is reduced to optimize the ensemble tree and minimize errors Eq. 3

$$L^{(t)} = \sum_{i=1}^{n} l(y_i, \hat{y}_i^{(t-1)} + f_t(x_i)) + \Omega(f_t) \tag{3}$$

Assuming $\hat{y}_i$ is the predicted value, and y_i is the observed value, l is a convex function applied to measure the discrepancy between observed and predicted outcomes. To minimize errors, iteration numbers *(t)* are applied, and the regularization term for the framework of the regression tree is defined as Eq. 4.

$$\Omega(f_k) = \gamma T + \frac{1}{2}\lambda \|w\|^2 \tag{4}$$

RF

Svetnik introduced the random forest regression model as an enhanced regression approach with classification capabilities[70,71]. The algorithm generates multiple decision trees by randomly sampling data points to construct its predictions. These decision trees are trained using distinct combinations of features and data subsets, culminating in a diverse ensemble of models. When integrated, this ensemble delivers precise predictions. By employing this ensemble learning approach, the algorithm minimizes the risk of overfitting and enhances its generalization capabilities. In RF regression, predictions are generated by constructing multiple decision trees, and the final output is determined by calculating the mean of the individual tree predictions. Figure 4 presents an overview of the RF algorithm's framework. The regression equation utilized to analyze the RF method is summarized below (Eq. 5)[72]:

$$M(x) = \frac{1}{N}\sum_{i=1}^{n}(y_i(x, \theta_n) \tag{5}$$

FBIO

Machine learning methods have been combined with metaheuristic optimization techniques to predict various factors, such as the Whale Optimization Algorithm, genetic algorithm, and particle swarm optimization[73,74]. The FBIO method distinguishes itself from other ways by eliminating the need to set internal factors. Instead, the optimization process is executed by adjusting iteration values and population sizes[75].

Therefore, the FBIO method can be a new approach to building an accurate model to estimate plastic concrete characteristics. It was originally introduced by Chou and Nguyen[76] as a mathematical problem-solving technique inspired by the simulation of police forces' forensic investigation activities. In this model, the search area represents the extent of the officer's query, and the term "culprit" denotes an optimal reply. The number of cooperating authorities determines the size of the community under examination. The level of complexity determines how much can be invested. Soon after the crime evidence is turned over to the FBIO base, the optimization process starts and stops when the culprit is taken to arrest. The FBI strategy is split into two phases: Stage P shows the track team's operations with the police. At the same time, Stage I analyzes the event and directs the inspection team (Fig. 5).

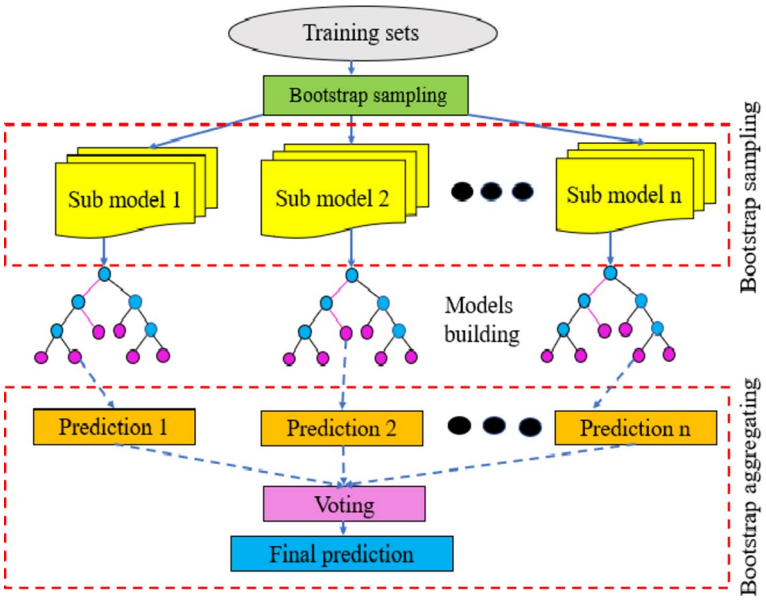

Fig. 4. The schematic flowchart of RF.

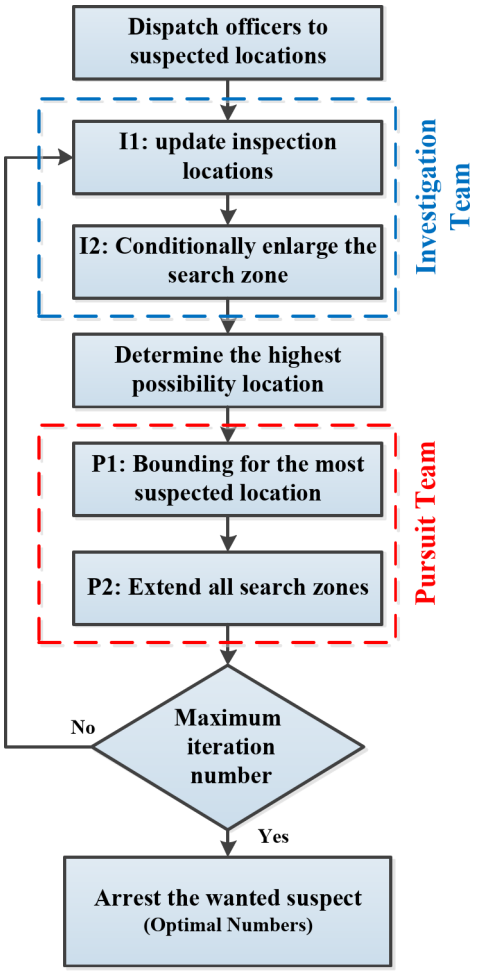

Fig. 5. The general process of FBIO.

The application process

Specifics of data gathering

The database employed in this study comprises 115, 158, and 119 datasets for tensile strength, elastic module, and slump[12,14,19,26,70,77–84].

Elwell and Fu[85] proposed UNESCO conversion factors to homogenize cylindrical and cubic values. As effective variables for BPC properties, this research examined the following variables: contents of gravel, bentonite, silty clay, curing time, sand, cement, and water. As shown Fig. 6, the intended graph distribution is not uniform, so the developed models apply to a wide range of target data[86]. A lower correlation is observed between negative and positive values in the overall model variables, as shown Fig. 7. In addition, according to the correlation heat map analysis, water, gravel, and curing time have a greater positive impact on the S, TS, and E of BPC, respectively.

Before modeling, the data were randomly split into testing (30%) and training (70%) parts. Tables 1, 2 and 3 display the statistical characteristics of the output and input variables for the testing and training data for S–BPC, TS–BPC, and E–BPC. A logical and technical range can be developed for each input variable by considering the highest value of the minimums and the lowest value of the maximums for each of the four data sets. In particular, these ranges are 295 to 875 kg/m^3 for gravel, 524 to 1305 kg/m^3 for sand, 0 to 260 kg/m^3 for silty clay, 80 to 252 kg/m^3 for cement, 18 to 100 kg/m^3 for bentonite; 260 to 500 kg/m^3 for water; and 7 to 180 days for curing time. Tables 1, 2 and 3 allow you to identify extreme data points (maximum and minimum), data centers (mean and median), data spread (standard deviation and variance), and distribution shapes (skewness and kurtosis)[86]. Moreover, the diversity among databases and the ability of models developed on them to generalize are illustrated by the diverse alterations observed in each of the outputs[17].

Model efficiency assessment specifications

Several error metrics were employed to assess the accuracy of the models (Eqs. (6–11)). These variables are R^2, MAE, RMSE, MAPE, a20-index, and OBJ[18]. These statistical metrics are summarized as follows:

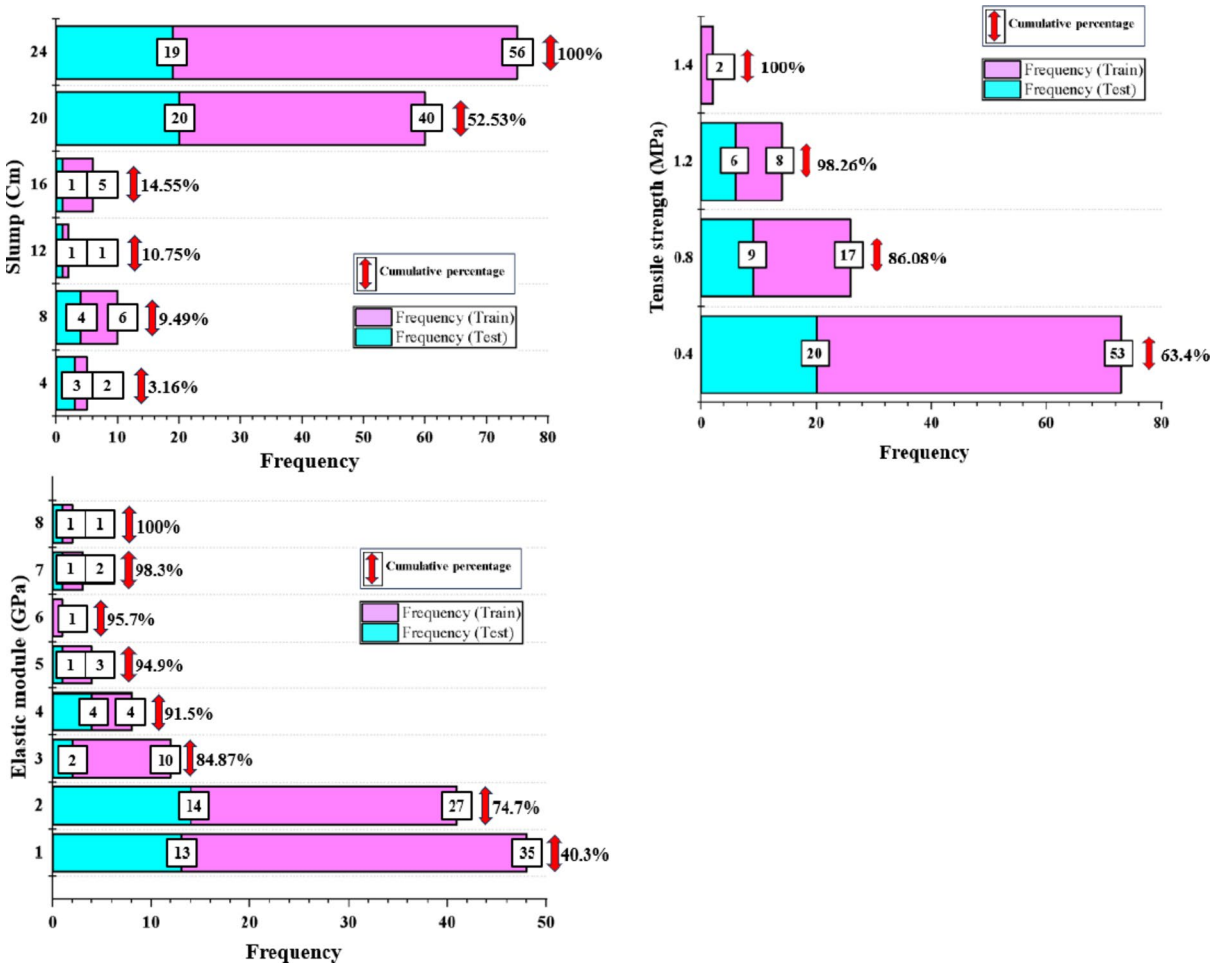

Fig. 6. Frequency histogram of output targets.

$$R^2 = \left[\frac{\sum_{i=1}^{N} (Y_{obs} - \overline{Y}_{obs})(Y_{pre} - \overline{Y}_{pre})}{\sqrt{\sum_{i=1}^{N} (Y_{obs} - \overline{Y}_{obs})^2 \sum_{i=1}^{N} (Y_{pre} - \overline{Y}_{pre})^2}} \right]^2 \tag{6}$$

$$MAE = \frac{\sum_{i=1}^{N} |Y_{pre} - Y_{obs}|}{N} \tag{7}$$

$$MAPE = \frac{\sum_{i=1}^{N} |Y_{pre} - Y_{obs}|}{\sum_{i=1}^{N} Y_{obs}} \times 100 \tag{8}$$

$$RMSE = \sqrt{\frac{1}{N} \sum_{i=1}^{N} (Y_{pre} - Y_{obs})^2} \tag{9}$$

$$OBJ = \left(\frac{N_{tr}}{N_{all}} . \frac{RMSE_{tr} + MAE_{tr}}{R_{tr}^2 + 1}\right) + \left(\frac{N_{tst}}{N_{all}} . \frac{RMSE_{tst} + MAE_{tst}}{R_{tst}^2 + 1}\right) \tag{10}$$

$$a20 - index = \frac{m20}{N} \tag{11}$$

When N is the number of records, Y_{pre} and Y_{obs} show the predicted and actual values, and the bar items over the parameters indicate the average rate; The variable m20 shows the quantity of the records where the Y_{obs}/Y_{pre} ratio ranges from 0.80 to 1.20; the terms "tst" applied for testing and "tr" applied for training data, accordingly.

Fig. 7. Pearson correlation Coefficients for S, TS, and E.

Algorithms for hybrid ensemble learners

The FBIO was used in this study to determine the ideal values using the given criteria to set the first random values (Table 4). After these statistics were entered into EL approaches and the EL algorithms were trained using the training dataset, the objective function was determined to be the average RMSE of both data (test and train). Figure 8 provides a summary of the various EL- FBIO approaches. Tables 5, 6 and 7 present the multiple meta-parameter values optimized for the S-PC, TS-PC, and E-BPC models.

Model prediction accuracy study

Because of a higher R^2-value and fewer scattered spots, the GBRT-FBIO approach outperforms conventional E-BPC models in both phases of testing and training, as shown in Fig. 9. Furthermore, with just a minor deviation from GBRT-FBIO, the given low values of RMSE and MAE in XGB-FBIO model demonstrate the excellent accuracy and dependability in the procedures of TS-BPC (Fig. 10). A20-index is a new significant engineering parameter that determines how many specimens have expected values at most 20% off from observed values[87]. With an a20-index of 0.916 during the testing step and 1.00 during training, XGB- FBIO is the most accurate predictor of S-BPC. Furthermore, with an a20-index of 0.833 and 0.963 throughout the testing and training step, the RF- FBIO had the lowest desire to perform well for S-BPC (Fig. 11).

Different statistical indicators were evaluated for training and testing datasets to assess the precision of the proposed forecasting models. Table 8 shows the results for different statistical parameters. In the S-BPC training phase, ADB is 0.32, 0.02, and 0.76 cm lower than GBRT, XGB, and RF in terms of RMSE, while in the testing phase, XGB outperformed ADB, GBRT, and RF by 0.05, 0.07, and 0.53 cm of difference in RMSE, respectively. In addition, XGB surpasses other TS-BPC models with MAPE values of 0.3 and 0.12%, respectively, for the training and testing stages. A comparison of R^2 values for E-BPC models reveals that GBRT (99.9% for train and 97.2% for test) and RF (94.1% for train and 87% for test) models exhibit the highest and lowest prediction accuracy, respectively.

The OBJ enables the combination of numerous statistical indicators for testing and training data to assess the model's generalizability[88]. The OBJ high values imply that a method performs badly compared to other ways[89].

Statistic	Gravel	Sand	Silty clay	Cement	Bentonite	Water	Slump
Training data: 110							
Minimum	0	509	0	72	15	152.1	0.8
Maximum	926	1372	260	289	168	520	23
Mean	672.9	826.3	33.9	176.5	46.2	347.1	18.3
Median	770.5	750	0	195	39	340	20
Standard deviation	225.4	212.7	75.6	49.7	27.9	70.7	4.3
Variance	50847.1	45273.8	5723.8	2470.7	780.7	5011.3	19.2
Skewness	−1.5	1.55	1.86	−0.08	2.3	−0.2	−2.4
Kurtosis	1.2	1.13	1.67	−0.8	6.6	0.6	6
Testing data: 48							
Minimum	0	441	0	90	15	162	1
Maximum	912	1499	225	300	140	500	24
Mean	729.9	775.8	32.8	191.6	42.2	333.6	16.9
Median	774.5	750	0	200	36.4	330	19
Standard deviation	169.6	189.1	74.5	50.1	24.7	62.6	5.7
Variance	28768.3	35759.4	5553	2515.8	610.3	3924.5	33.3
Skewness	−2.7	2.4	1.8	0.05	2.1	−0.3	−1.7
Kurtosis	8.2	6.5	1.7	−0.4	5.1	1.16	1.7

Table 1. Comprehensive statistics for both testing and training data related to S-BPC.

Statistic	Gravel	Sand	Silty clay	Cement	Bentonite	Water	Curing time	Tensile strength
Training data: 80								
Minimum	295	590	0	50	18	152.1	28	0.06
Maximum	875	1305	350	252	320	500	180	1.3
Mean	625.9	851.8	144.5	142.2	69.7	351.5	59.2	0.3
Median	673.5	775	180	130	58	370	28	0.2
Standard deviation	192.5	253.5	109.4	45.2	43.9	78.6	38.6	0.2
Variance	37072.2	64308.6	11973.8	2043.6	1927.8	6191.2	1492.5	0.07
Skewness	−0.7	1	−0.3	0.7	2.7	−1	1.1	1.4
Kurtosis	−0.7	−0.5	−1.3	0.3	12.5	0.6	1.2	1.7
Testing data: 35								
Minimum	295	524	0	72	18	152.1	28	0.08
Maximum	875	1305	380	224	168	481.4	90	1
Mean	670.8	816.9	144	132.9	67.3	328.4	59.8	0.4
Median	710	766	180	120	70	340.4	90	0.3
Standard deviation	184.6	237.8	123	34.6	37	78.3	31.4	0.2
Variance	34082.4	56593.8	15137.9	1201.2	1374.3	6142.7	988.4	0.07
Skewness	−1.1	1.2	0.05	1.1	1.2	−0.4	−0.05	0.6
Kurtosis	0.1	0.3	−0.1.1	1	1.6	−0.3	−2.1	−1

Table 2. Comprehensive statistics for both testing and training data related to TS-BPC.

The best efficiency for the GBRT method for E-BPC is presented in Fig. 12, with an OBJ of 0.275 and 0.097%. Furthermore, the RF method performs the worst S, TS, E -BPC given the OBJ quantities of 0.912%, 0.058%, and 0.369%, respectively.

The Nash-Sutcliffe efficiency (NSE) and the scatter index (SI) coefficient were used as supplementary validation tests for the models by Eqs. (12)-(13).

$$SI = \frac{RMSE}{\overline{Y}_{obs}} \tag{12}$$

$$NSE = 1 - \frac{\sum_{i=1}^{N} (Y_{pre} - Y_{obs})^2}{\sum_{i=1}^{N} (Y_{obs} - \overline{Y}_{obs})^2} \tag{13}$$

Statistic	Gravel	Sand	Silty clay	Cement	Bentonite	Water	Curing time	Elastic module
Training data: 83								
Minimum	0	509	0	80	14.8	260	7	0.097
Maximum	1547.7	1407	380	300	100	495	180	7.5
Mean	845.5	817.8	96.8	171.9	47.4	362.9	55.3	1.6
Median	755	704.3	0	156	44	360	28	1
Standard deviation	337.1	271.1	123.4	55.9	19.5	48.5	38.3	1.4
Variance	113658.9	73507.9	15246.1	3134.1	383	2354.8	1469.2	2.1
Skewness	1	1.2	0.8	0.5	0.4	0.4	1.3	2.2
Kurtosis	0.3	−0.02	−0.7	−0.8	−0.6	0.1	1.7	5.1
Testing data: 36								
Minimum	0	604.5	0	100	16	296	7	0.1
Maximum	1519.6	1499	330	330	100	726	90	7.8
Mean	850.1	921.6	68	170.3	43.6	364.7	50.9	1.7
Median	790	790	0	160	40	338	28	1.1
Standard deviation	425	290.6	108.9	57.4	17.3	77	31.9	1.6
Variance	180630.5	84499.8	11867.5	3296.1	301.7	5934.7	1021.3	2.7
Skewness	0.08	−0.7	1.1	0.9	1.1	3.3	0.3	2.1
Kurtosis	−0.1	−1.1	−0.1	0.2	1.8	13.9	−1.7	4.7

Table 3. Comprehensive statistics for both testing and training data related to E-BPC.

Parameters	Considered range	Parameters	Considered range
Number of estimators	[5,200]	Max_samples	[0.1,1]
Min_samples_split	RF: [1,10] Other methods: [1e-10,1]	lu_ns	[2,150]
Min_samples _leaf	RF: [1,10] Other methods: [1e-10,1]	lu_max_d	[2,100]
Max_depth	[2,500]	lu_max_mlf	[2,100]
Max_features	[1, maximum number of variables]	lu_lr	[0.0001,1]
Max_ leaf_nodes	[2,500]	lu_gamma	[0,10]
Ccp_alpha	[0,1]	lu_gamma	[0,10]
Min_weight_fraction_leaf	[0,0.5]	lu_min_cw	[0,1]
Learning rate	[0.001,3]	lu_subsample	[0.5,1]
Alpha	[0.001,0.99]	lu_subsample_bt	[0.5,1]
Subsample	[1e-6,1]	reg_lambda	[0.01,2]

Table 4. Different meta-parameter ranges used in the optimization process.

In which the bar items over the associated digits represent the average of each value, N represents the records number, and Y_{obs} refer to the observed and Y_{pre} represent anticipated quantities. A model's predictive accuracy is regarded as excellent if NSE is more than 0.75 or SI is less than 0.1 or good if NSE is between 0.65 and 0.75 or SI is between 0.1 and 0.2. However, it is fair if the NSE value is between 0.5 and 0.65 or the SI is between 0.2 and 0.3[18]. As seen in Fig. 13, all methods have SI rates less than 0.2, indicating that they are excellent or good predictors of plastic concrete. The results also show that all methods had NSE rates greater than 0.75, indicating the EL-FBIO models' "excellent" accuracy in forecasting output values (Fig. 14).

The effectiveness of each design was evaluated using Taylor's diagram presented in Fig. 15. To compare the anticipated outcomes with the actual values, three statistical measures (RMSE, STD, and R^2) were used. The standard deviation is shown through a circle connecting the plot's horizontal and vertical axes; the horizontal green dots indicate RMSE, and the blue line shows the values of R^2. As a result, among all techniques for S, TS, and E-BPC, the GBRT-FBIO and XGB methods have the top performance.

ML and EL models can accurately predict BPC strength and workability properties, as reported by several studies[19,26]. According to the R^2 comparison, the GBRT method for E and XGB methods for TS and Slump outperformed all existing models during the testing and training levels (Table 9). As a result, EL methods are more practical and more effective in generalizing BPC characteristics, thus saving time and resources.

Important features using shapley values

SHAP is a game-theoretic approach designed to describe the result of machine-learning methods[90]. SHAP presents the feature's contribution to the model's output, offering a more interpretable and transparent understanding of the model's decision-making process. In the ensuing sections, we thoroughly analyze the outcomes in the proposed predicting structure, designed to interpret and comprehend the results of the probabilistic predicting

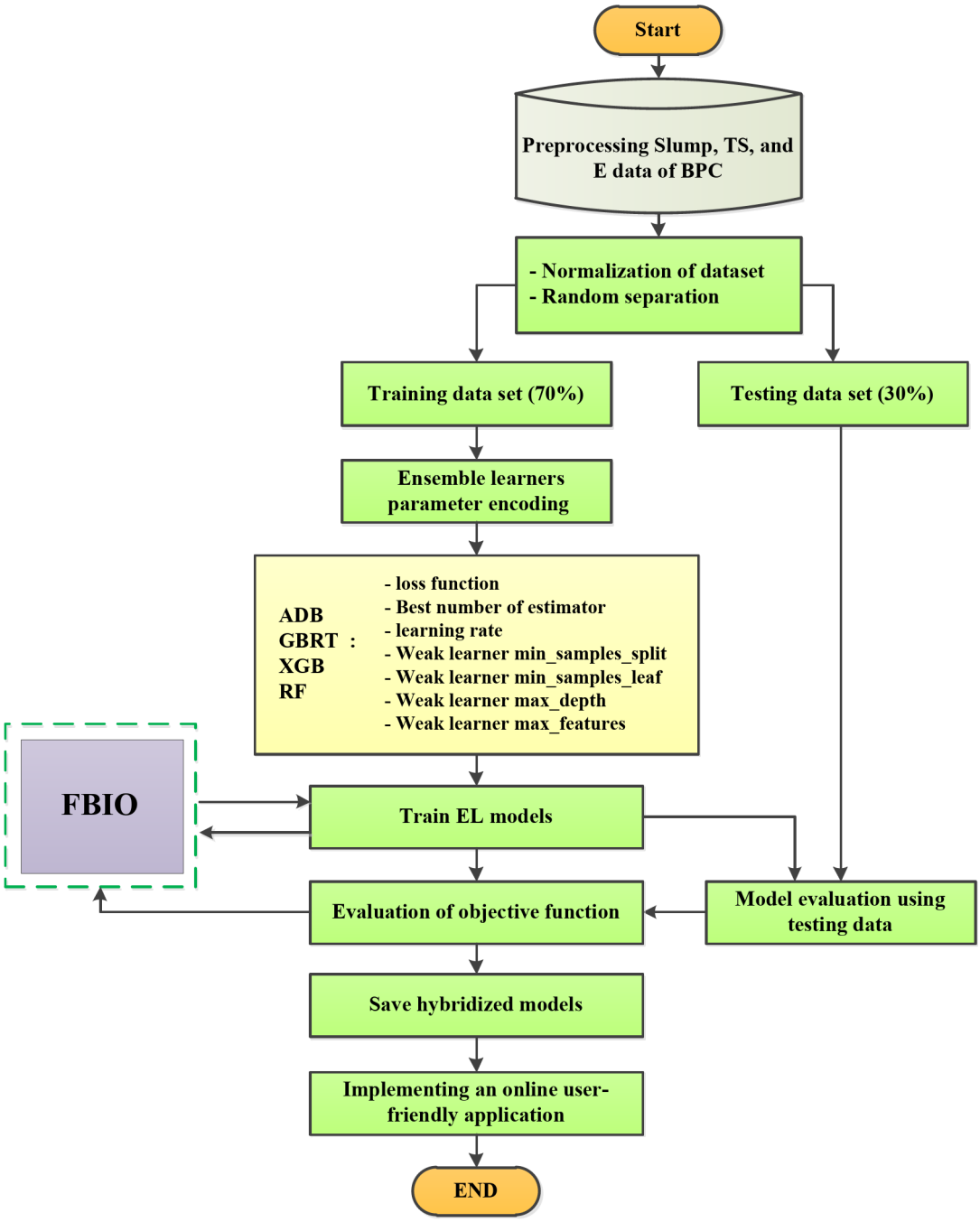

Fig. 8. An overview of the modeling process in this study.

model. Our initial focus is point forecasts, specifically examining how the developed model utilizes various features to make predictions. The SHAP method is employed for explanations, covering S, TS, and E. Figure 16 illustrates the average contribution of each feature, with each bar plot representing the importance of a specific property. Cement and water play significant roles in TS models, contributing more substantially. The primary contributors for E are curing time and cement, with mean SHAP values of + 0.18 and + 0.12, respectively. Water (+ 0.11) and sand (+ 0.09) make more notable contributions in the slump model. Silt (for E and S) and bentonite (for TS) exhibit minimal impact on the output of the models.

Each dot in Fig. 17 represents a distinct forecasting, and its location along the x-axis signifies that attribute's impact on the model's output. Furthermore, each dot's color corresponds to a feature value (varies from blue to red), emphasizing the relative contributions of different feature values to the final result. The long tails show highly significant characteristics. The dots' vertical distribution suggests more findings with comparable effects. These SHAP summary graphs in such a setting include details on the number of reports with those qualities and the size and direction of each feature's effect.

Parameters	Models			
	ADB-FBIO	GBRT- FBIO	XGB- FBIO	RF- FBIO
Number of estimators	29	75	64	10
Min_samples_split	0.0031	0.04	-	2
Min_samples _leaf	0.0032	0.02	-	1
Max_depth	268	120	500	446
Max_features	1	3	-	1
Max_ leaf_nodes	363	8	39	154
Ccp_alpha	0	6.74e-05	-	0
Min_weight_fraction_leaf	1e-8	0.02	-	0
Learning rate	0.5	0.35	0.78	-
Alpha	-	0.18	-	-
Subsample	-	0.5	0.5	-
Max_samples	-	-	-	0.89
Gamma	-	-	1	-
Min_child_weight	-	-	0.17	-
Reg_lambda	-	-	1.27	-
Colsample_bytree	-	-	0.88	-

Table 5. Optimized parameter values for S-BPC.

Parameters	Models			
	ADB-FBIO	GBRT- FBIO	XGB- FBIO	RF- FBIO
Number of estimators	28	47	185	128
Min_samples_split	0.04	0.05	-	4
Min_samples _leaf	0.01	0.02	-	1
Max_depth	64	131	472	481
Max_features	1	3	-	1
Max_ leaf_nodes	72	8	500	197
Ccp_alpha	1.62	1.14e-05	-	0
Min_weight_fraction_leaf	0.0003	0.005	-	0
Learning rate	0.25	0.36	0.61	-
Alpha	-	0.18	-	-
Subsample	-	0.79	0.91	-
Max_samples	-	-	-	0.95
Gamma	-	-	4.75	-
Min_child_weight	-	-	0.37	-
Reg_lambda	-	-	1.91	-
Colsample_bytree	-	-	0.79	-

Table 6. Optimized parameter values for TS-BPC.

A heatmap of SHAP values across all input variables is shown in Fig. 18. Slump, TS, and E were shown on top as functions of all variables. The ranges of SHAP values, which show the impact on each model target, are depicted in various colors ranging from blue to red. For this heatmap, arbitrary sample pools equal to training data sets were chosen. For S-BPC samples below 15, on the left of the heatmap, the highest prediction (highest in f(x)) corresponds to an absolute red color for water, indicating that it has contributed most to the slump. Considering the intense 77 on the right side of the TS-BPC heatmap, water again appears to be one key input parameter. However, curing time and cement with a strong red color on the left side are essential factors when predicting E-BPC.

Online application of proposed BPC models

Models developed using EL-FBIO methods differ from classical regression methods as they do not simply relate inputs and outputs[91]. In this regard, implementing an online application makes it possible for researchers and practicing engineers, the end users of the proposed BPC models, to easily estimate values of mechanical and workability properties. In the past, several researchers have developed software using MATLAB Graphical User Interface (GUI) to predict the properties of different types of concrete[92,93]. There are several advantages to the developed online application: (i) results are available more quickly, and it provides a standard for an in-depth

Parameters	Models			
	ADB-FBIO	GBRT- FBIO	XGB- FBIO	RF- FBIO
Number of estimators	7	44	16	5
Min_samples_split	0.02	1.00e-08	-	2
Min_samples _leaf	0.002	0.003	-	1
Max_depth	227	298	254	499
Max_features	1	2	-	7
Max_ leaf_nodes	309	9	271	168
Ccp_alpha	0.00019	0	-	1.42
Min_weight_fraction_leaf	0.0018	0.02	-	0.0007
Learning rate	0.42	0.59	1.36	-
Alpha	-	0.05	-	-
Subsample	-	0.98	0.85	-
Max_samples	-	-	-	0.97
Gamma	-	-	0.0003	-
Min_child_weight	-	-	0.81	-
Reg_lambda	-	-	1.007	-
Colsample_bytree	-	-	0.88	-

Table 7. Optimized parameter values for E-BPC.

investigation of mix designs; (ii) reducing production costs while ensuring the safety of concrete designs and quality concerns as well, it allows to determine if a mix design is reasonable; and (iii) in addition to being easy to use, it will reduce human errors in calculations[94]. Free online access is also provided[95]. This application enables engineers and researchers to obtain a relatively accurate prediction of the strength and workability parameters of BPC at their project site in simple steps.

Limitations and future perspectives

The proposed ensemble learning models hybridized with Forensic-Based Investigation Optimization (FBIO) demonstrated high predictive accuracy, but certain limitations must be addressed. The relatively small dataset sizes of 158, 115, and 119 records for slump, tensile strength, and elastic modulus, respectively, may restrict the generalizability of the models to broader scenarios and diverse environmental conditions. Despite the application of SHAP analysis to provide insights into feature importance, the complexity of ensemble models may hinder their interpretability for non-specialist users. Additionally, the computational costs associated with FBIO-enhanced ensemble models for hyperparameter tuning and optimization may limit scalability for real-time applications or larger datasets. The reliance on datasets compiled from literature introduces potential biases that could impact the robustness of the models when applied to new or unseen data. To address these limitations, future studies should focus on expanding datasets to include more diverse material properties, environmental conditions, and testing protocols to enhance model robustness and generalizability. Simplifying models or integrating surrogate modeling techniques could improve interpretability without compromising accuracy. Advanced learning techniques such as deep neural networks (DNNs) and transfer learning could improve predictive performance and adaptability. Incorporating uncertainty quantification methods would enhance understanding of prediction reliability, especially for critical engineering applications. Finally, improving computational efficiency through optimization techniques like Bayesian optimization or genetic algorithms would facilitate real-time model implementation, enabling practical use in broader applications. Addressing these limitations and pursuing these potential improvements will significantly enhance the usability, accuracy, and efficiency of predictive models for BPC.

Conclusion

This study significantly advances the understanding and prediction of BPC properties by developing hybridized ensemble learning models enhanced with FBIO. Using datasets containing 158, 115, and 119 records for S, TS, and E, respectively, the proposed models achieved superior predictive accuracy, reducing the need for labor-intensive and costly experimental testing. A summary of the findings is provided below:

1. The study successfully introduced hybrid ensemble learning models, specifically GBRT, XGB, ADB, and RF, optimized with FBIO, which outperformed traditional approaches in predicting BPC properties.
2. Among the models, GBRT-FBIO achieved an R^2 value of 97.2% for elastic modulus predictions. XGB-FBIO attained an R^2 value of 97.7% and 96.6% for tensile strength and slump predictions, respectively.
3. GBRT-FBIO significantly reduced RMSE to 0.278 for elastic modulus predictions.
4. The study introduced new performance indicators, such as the a20-index, which revealed that XGB-FBIO achieved a20-indices of 91.6% for slump predictions, highlighting its high accuracy and reliability.
5. The models demonstrated scalability for real-world applications. XGB-FBIO and GBRT-FBIO achieved OBJ values of 0.012 and 0.097 for tensile strength and elastic modulus predictions, validating their reliability across diverse scenarios.

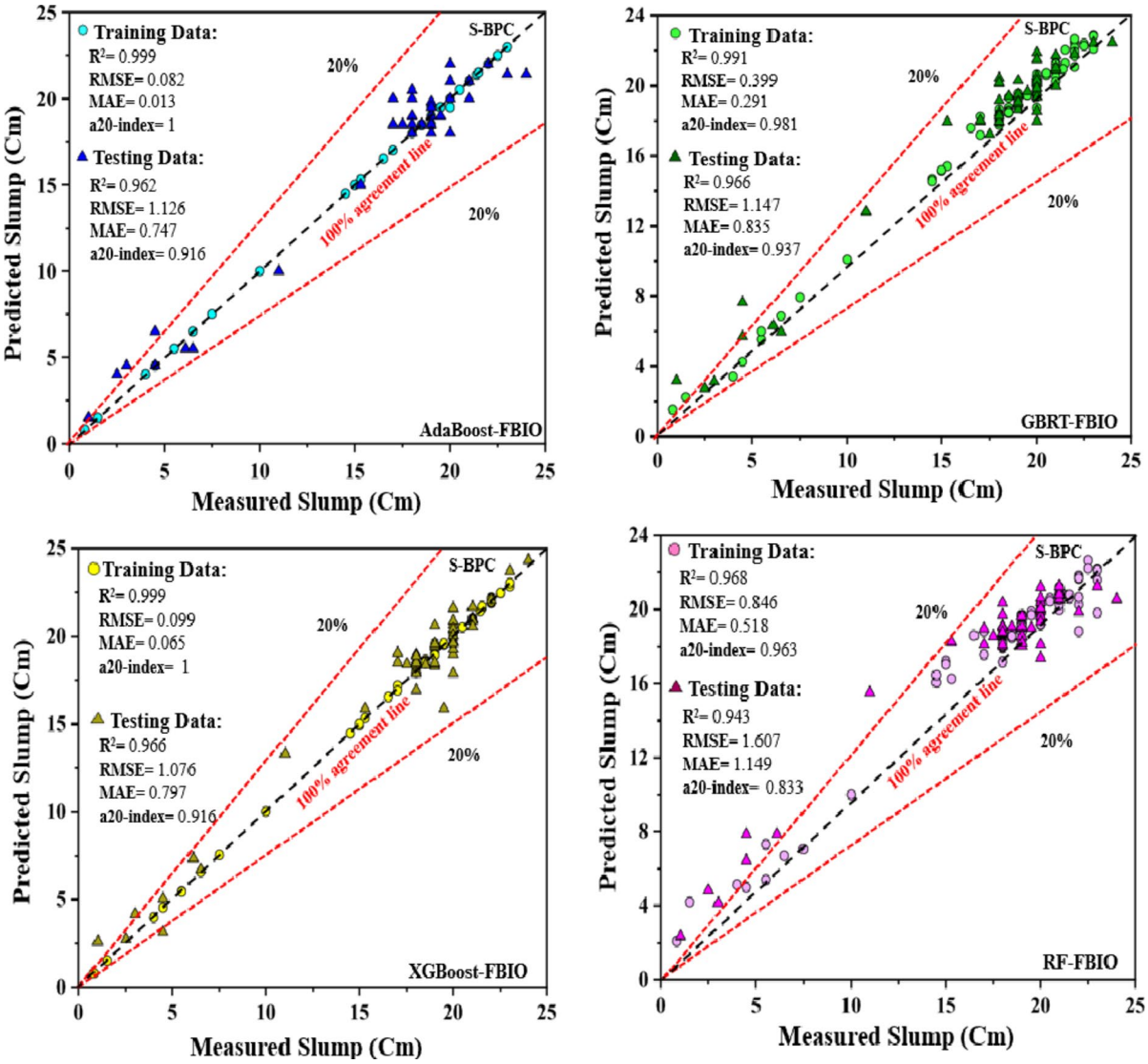

Fig. 9. Measured versus expected scattering dots in the E-BPC phases.

6. SHAP analysis revealed water as the most critical factor for slump, contributing a mean impact of + 0.11, while curing time was the primary determinant for tensile strength and elastic modulus, with mean contributions of + 0.18 and + 0.12, respectively.
7. The study developed an online user-friendly platform for predicting BPC properties, which reduces reliance on costly experimental tests and enables faster mix design evaluations directly at project sites.

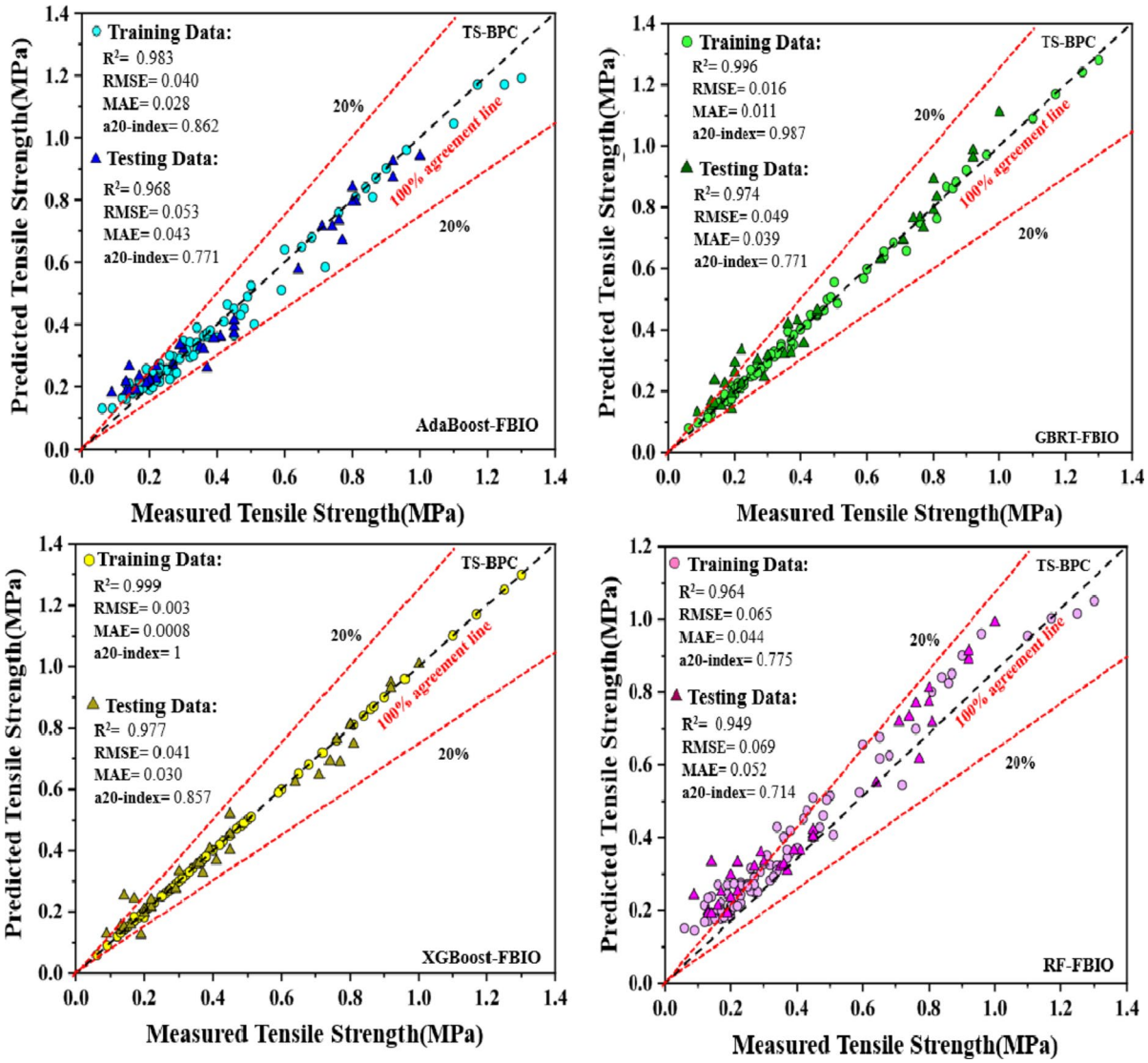

Fig. 10. Measured versus expected scattering dots in the TS-BPC phases.

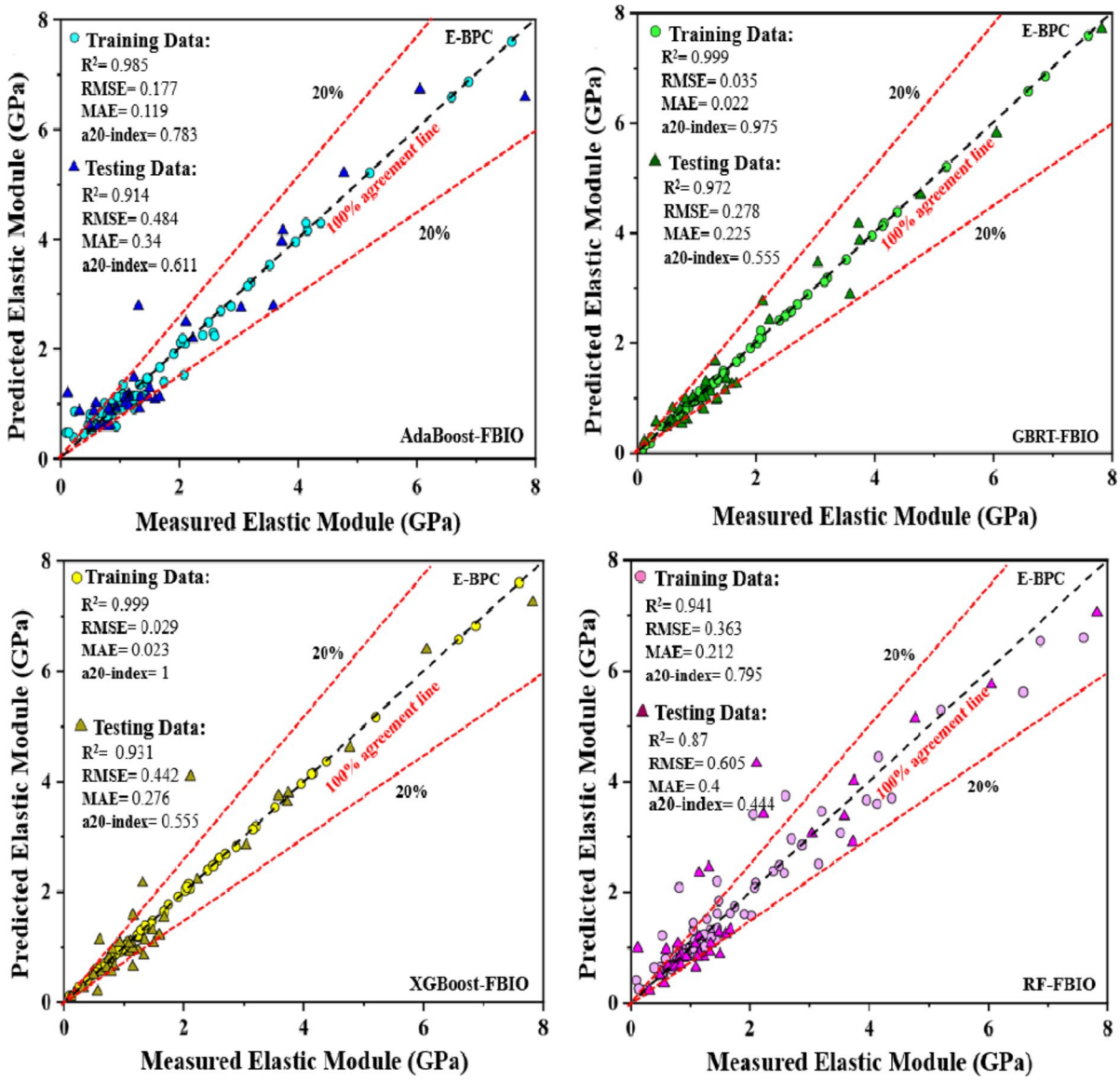

Fig. 11. Measured versus expected scattering dots in the S-BPC phases.

Models	Training				Testing			
	R^2	RMSE	MAE	MAPE	R^2	RMSE	MAE	MAPE
S-BPC								
ADB- FBIO	0.999	0.082	0.013	0.0007	0.962	1.126	0.747	0.079
GBRT-FBIO	0.991	0.399	0.291	0.029	0.966	1.147	0.835	0.108
XGB- FBIO	0.999	0.099	0.065	0.003	0.966	1.076	0.797	0.094
RF- FBIO	0.968	0.846	0.518	0.061	0.943	1.607	1.149	0.144
TS-BPC								
ADB- FBIO	0.983	0.040	0.028	0.116	0.968	0.053	0.043	0.181
GBRT-FBIO	0.996	0.016	0.011	0.04	0.974	0.049	0.039	0.146
XGB- FBIO	0.999	0.003	0.0008	0.003	0.977	0.041	0.03	0.115
RF- FBIO	0.964	0.065	0.044	0.164	0.949	0.069	0.052	0.243
E-BPC								
ADB- FBIO	0.985	0.177	0.119	0.219	0.914	0.484	0.340	0.495
GBRT-FBIO	0.999	0.035	0.022	0.029	0.972	0.278	0.225	0.195
XGB- FBIO	0.999	0.029	0.023	0.028	0.931	0.442	0.276	0.220
RF- FBIO	0.941	0.363	0.212	0.195	0.870	0.605	0.400	0.458

Table 8. The precision and effectiveness of each EL-FBIO model.

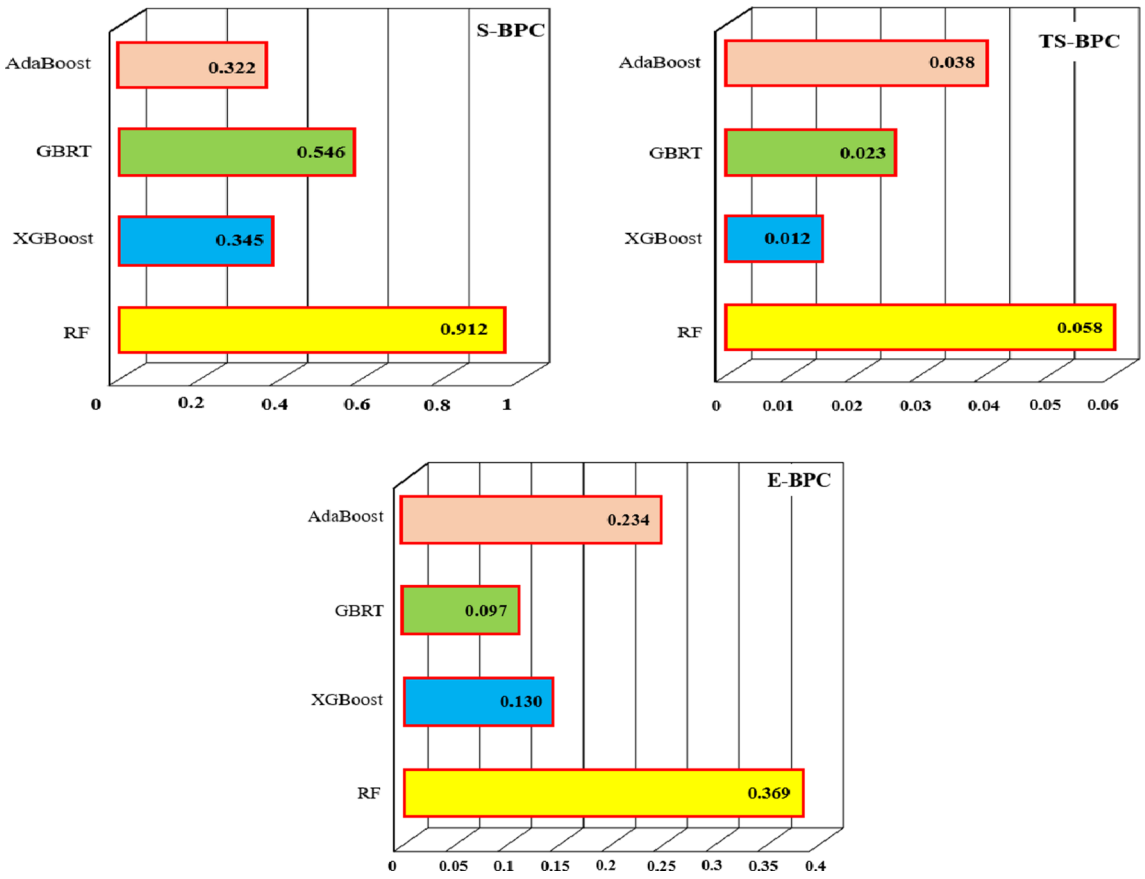

Fig. 12. OBJ values of different implemented FBIO models.

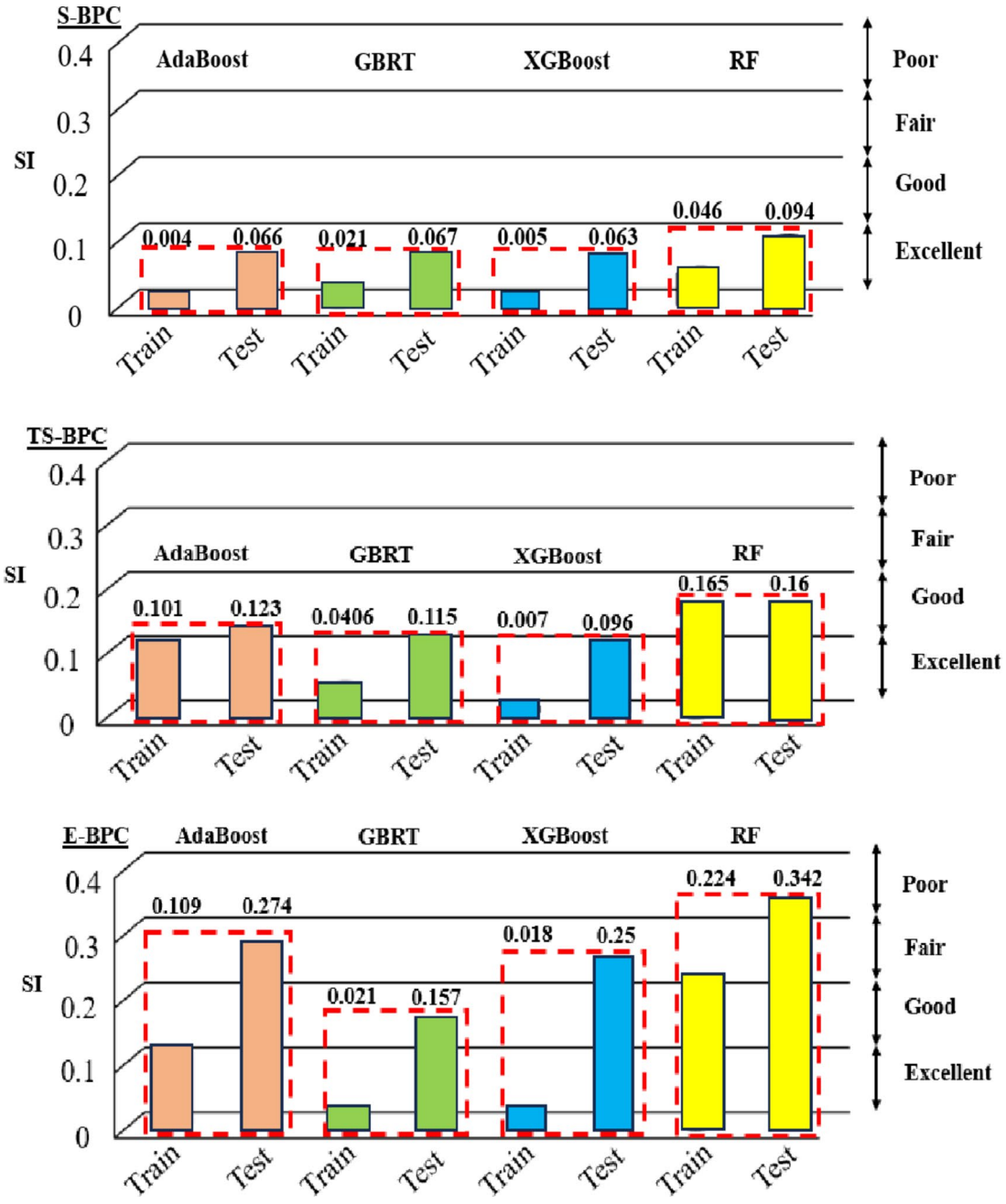

Fig. 13. Calculated SI values for FBIO models.

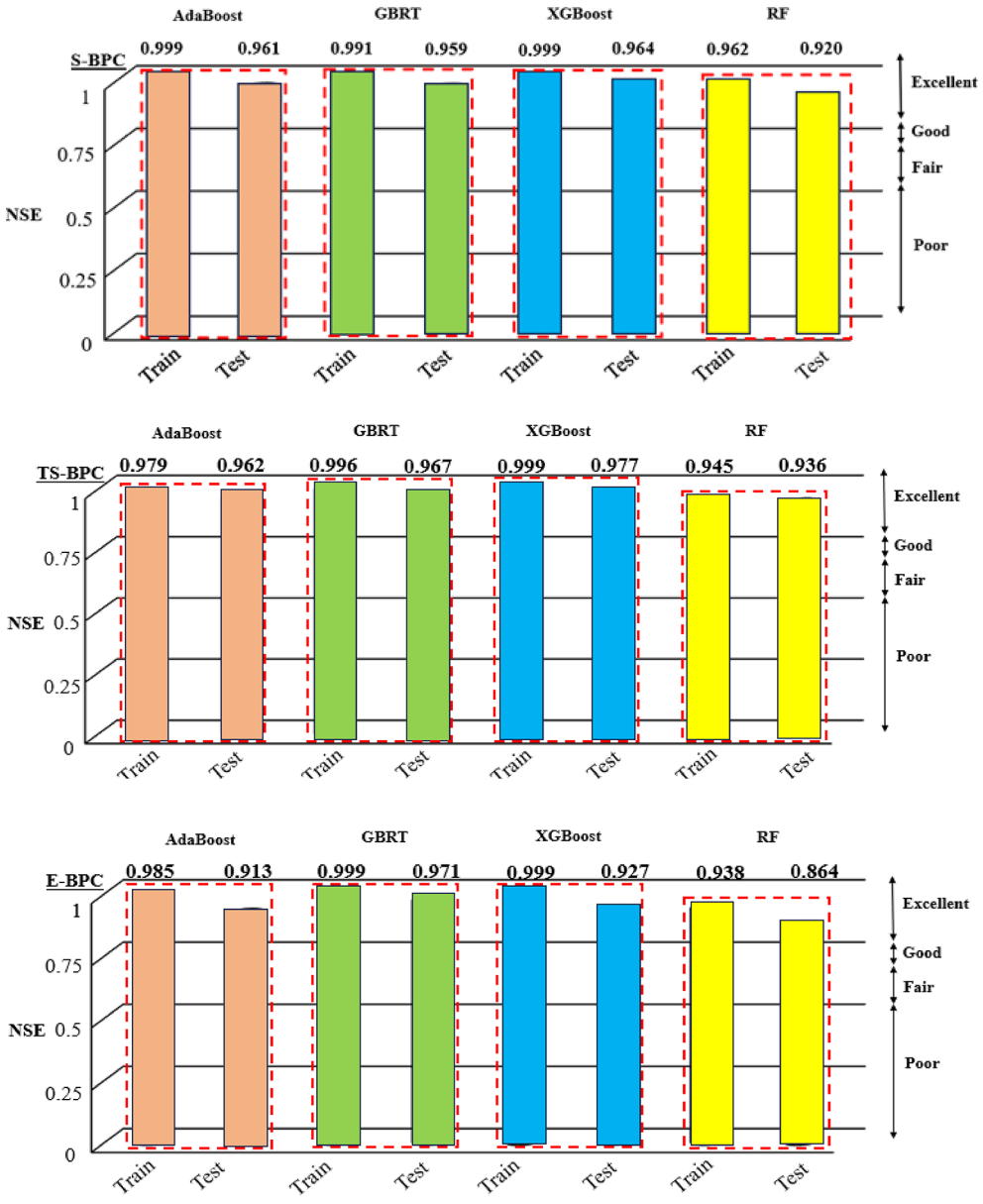

Fig. 14. Calculated NSE values for FBIO models.

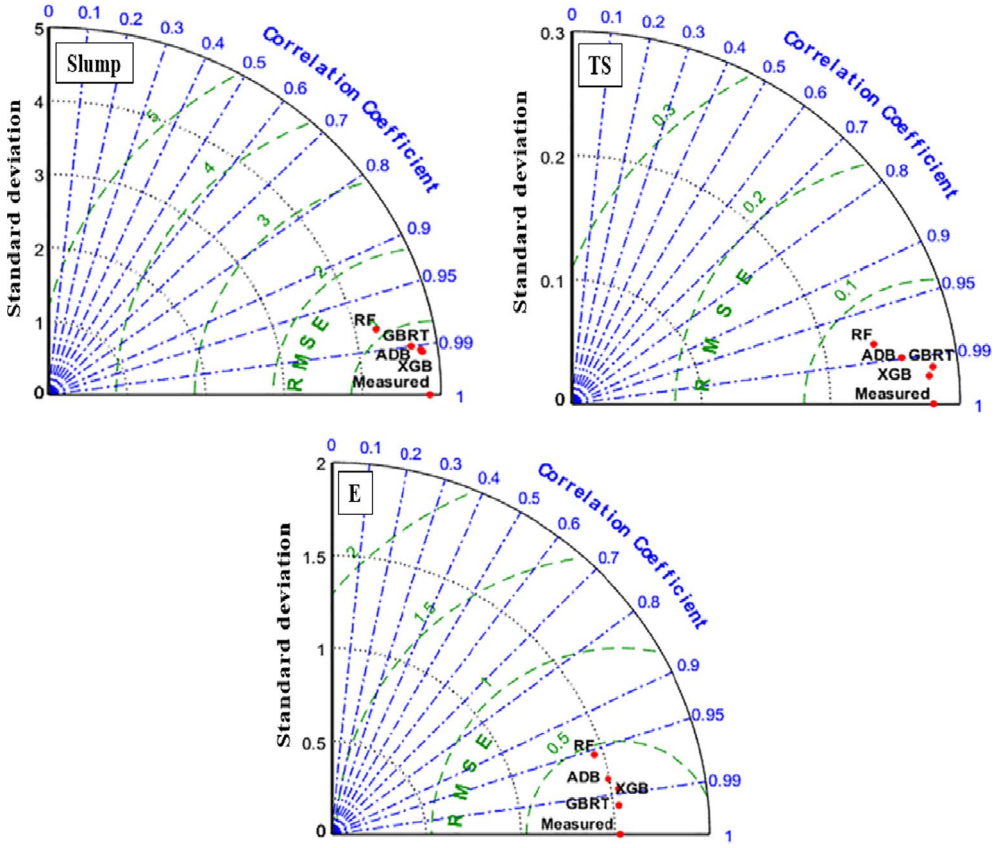

Fig. 15. Taylor graphs of several EL-FBIO models and traditional approaches.

Model	Year	Ref	Inputs No.	No. of Data	R^2		RMSE		MAE	
					Train	Test	Train	Test	Train	Test
Slump (cm)										
ANN	2019	Tavana Amlashi et al.[20]	6	158	0.963	0.935	0.961	1.168	0.668	0.772
MARS	2019	Tavana Amlashi et al.[20]	6	158	0.832	0.761	2.040	2.381	1.516	1.665
M5Tree	2019	Tavana Amlashi et al.[20]	6	158	0.893	0.858	1.814	1.803	1.422	1.273
ADB-FBIO	2024	This Study	6	158	0.999	0.962	0.082	1.126	0.013	0.747
GBRT-FBIO	2024	This Study	6	158	0.991	0.966	0.399	1.147	0.291	0.835
XGB-FBIO	2024	This Study	6	158	0.999	0.966	0.099	1.076	0.065	0.797
RF-FBIO	2024	This Study	6	158	0.968	0.943	0.846	1.607	0.518	1.149
TS (MPa)										
SVM	2020	Tavana Amlashi et al.[27]	8	107	0.999	0.968	0.003	0.048	-	-
ANN	2020	Tavana Amlashi et al.[27]	8	107	0.999	0.936	0.003	0.052	-	-
ANFIS	2020	Tavana Amlashi et al.[27]	8	107	0.959	0.932	0.033	0.057	-	-
ADB-FBIO	2024	This Study	7	115	0.983	0.968	0.040	0.053	0.028	0.043
GBRT-FBIO	2024	This Study	7	115	0.996	0.974	0.016	0.049	0.011	0.039
XGB-FBIO	2024	This Study	7	115	0.999	0.977	0.003	0.041	0.0008	0.03
RF-FBIO	2024	This Study	7	115	0.964	0.949	0.065	0.069	0.044	0.052
E (GPa)										
ANN	2019	Tavana Amlashi et al.[20]	7	119	0.964	0.918	0.280	0.472	0.229	0.293
MARS	2019	Tavana Amlashi et al.[20]	7	119	0.755	0.629	0.735	0.998	0.487	0.677
M5Tree	2019	Tavana Amlashi et al.[20]	7	119	0.753	0.803	0.769	0.765	0.486	0.510
ADB-FBIO	2024	This Study	7	119	0.985	0.914	0.177	0.484	0.119	0.340
GBRT-FBIO	2024	This Study	7	119	0.999	0.972	0.035	0.278	0.022	0.225
XGB-FBIO	2024	This Study	7	119	0.999	0.931	0.029	0.442	0.023	0.276
RF-FBIO	2024	This Study	7	119	0.941	0.870	0.363	0.605	0.212	0.400

Table 9. Comparing proposed EL models to those in the literature.

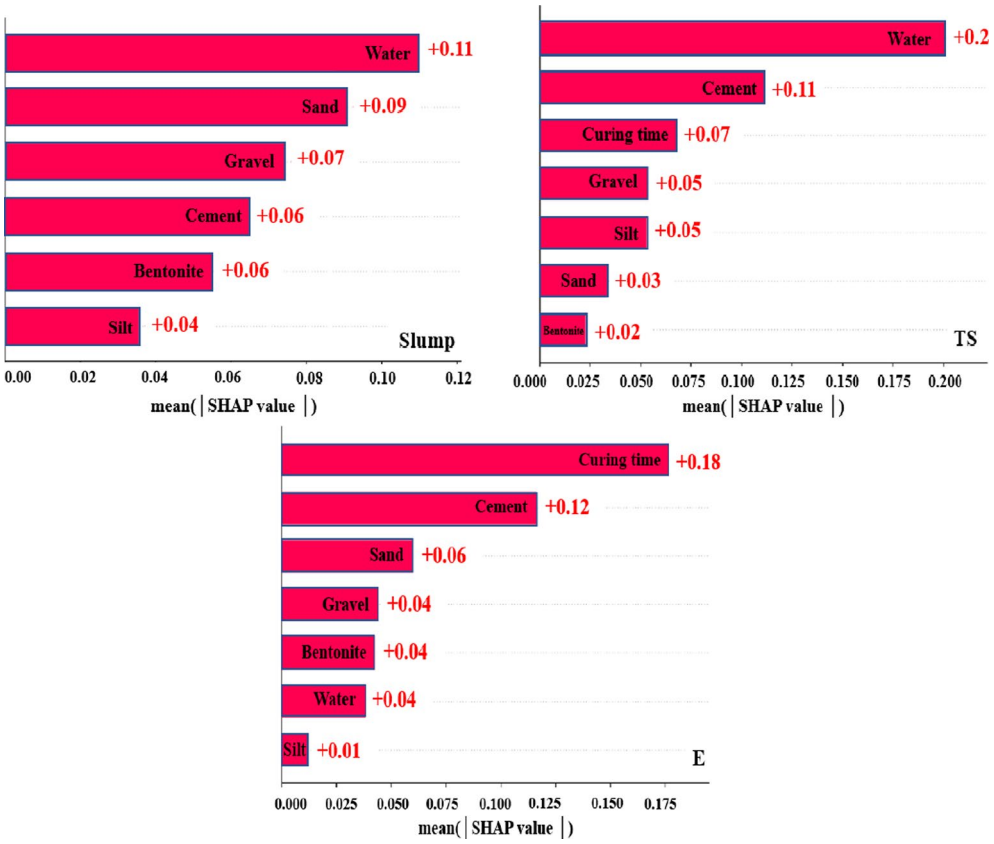

Fig. 16. Feature significance of the input variables.

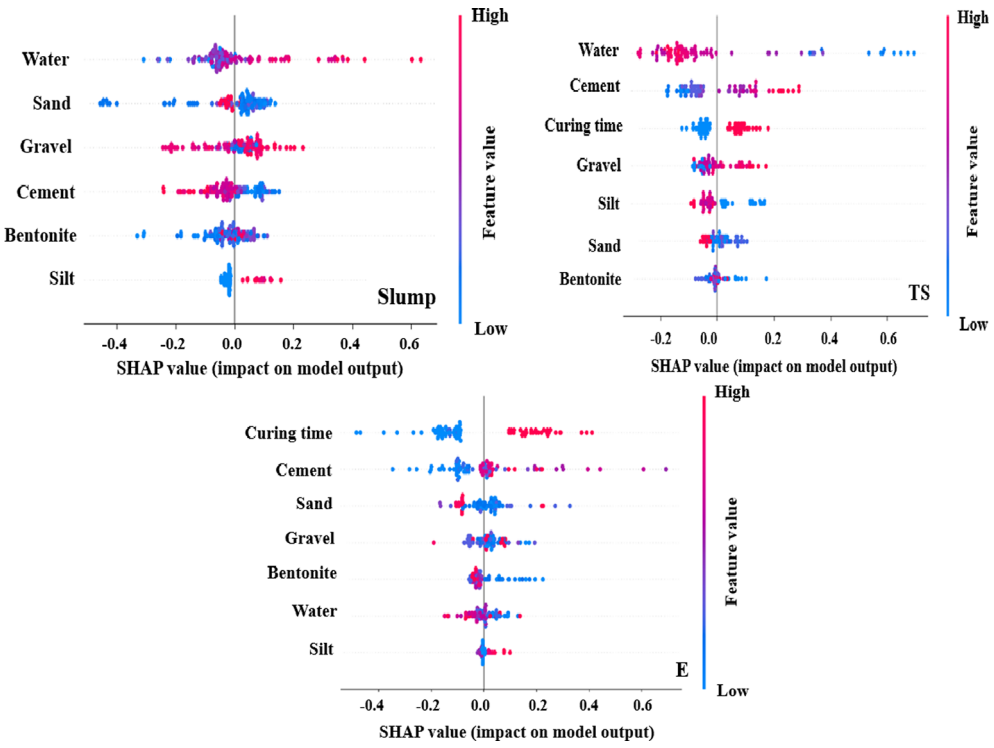

Fig. 17. Summary plot of the point predicting model.

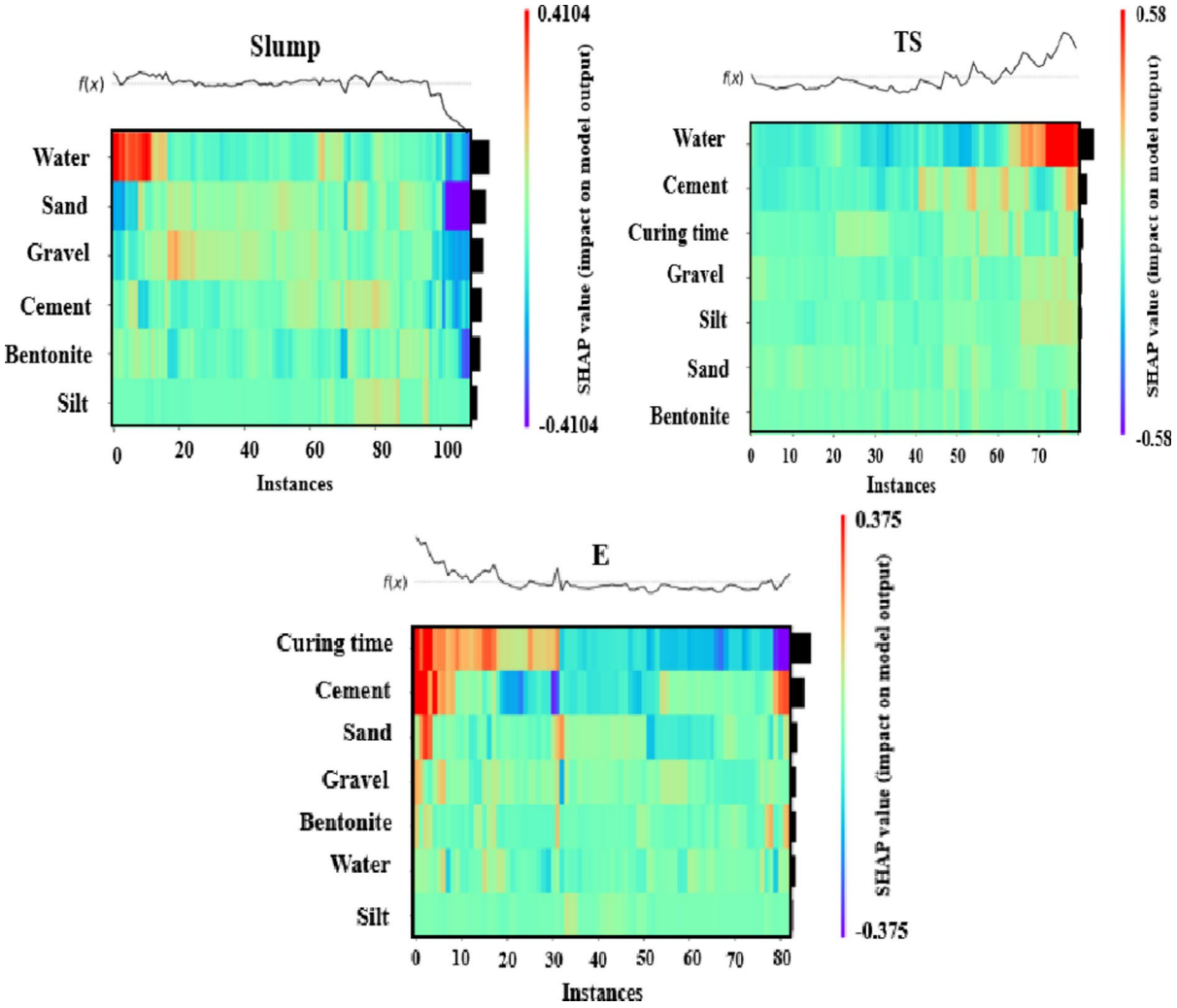

Fig. 18. SHAP values and function variations of each target.

Data availability

Data will be made available on request from the corresponding authors.

Received: 19 July 2024; Accepted: 26 February 2025
Published online: 05 March 2025

References

1. Keramati, M., Goodarzi, S., Moghadam, M., Ramesh, A. & H., & Evaluating the stress–strain behavior of MSW with landfill aging. *Int. J. Environ. Sci. Technol.* **16**, 6885–6894 (2019).
2. Pandey, G. & Madhuri, S. Heavy metals causing toxicity in animals and fishes. *Res. J. Anim. Veterinary Fish. Sci.* **2** (2), 17–23 (2014).
3. Tytła, M. Assessment of heavy metal pollution and potential ecological risk in sewage sludge from municipal wastewater treatment plant located in the most industrialized region in Poland—case study. *Int. J. Environ. Res. Public Health*. **16** (13), 2430 (2019).
4. Liu, Q., Zhou, Y., Lu, J. & Zhou, Y. Novel cyclodextrin-based adsorbents for removing pollutants from wastewater: A critical review. *Chemosphere* **241**, 125043 (2020).
5. Uddin, M. K. A review on the adsorption of heavy metals by clay minerals, with special focus on the past decade. *Chem. Eng. J.* **308**, 438–462 (2017).
6. Barakan, S. & Aghazadeh, V. The advantages of clay mineral modification methods for enhancing adsorption efficiency in wastewater treatment: a review. *Environ. Sci. Pollut. Res.* **28**, 2572–2599 (2021).
7. Hussain, S. T. & Ali, S. A. K. Removal of heavy metal by ion exchange using bentonite clay. *J. Ecol. Eng.* **22** (1), 104–111 (2021).
8. Thakur, A. K., Kumar, R., Chaudhari, P. & Shankar, R. *Removal of Heavy Metals Using Bentonite Clay and Inorganic Coagulants*47–69 (Removal of Emerging Contaminants Through Microbial Processes, 2021).
9. Kinoti, I. K., Karanja, E. M., Nthiga, E. W., M'thiruaine, C. M. & Marangu, J. M. *Review of clay-based Nanocomposites as Adsorbents for the Removal of Heavy Metals* (Journal of Chemistry, 2022).
10. Dhar, A. K., Himu, H. A., Bhattacharjee, M., Mostufa, M. G. & Parvin, F. Insights on applications of bentonite clays for the removal of dyes and heavy metals from wastewater: a review. *Environ. Sci. Pollut. Res.* **30** (3), 5440–5474 (2023).
11. Shubber, M. D. & Kebria, D. Y. Thermal recycling of bentonite waste as a novel and a low-cost adsorbent for heavy metals removal. *J. Ecol. Eng.*, **24**(5). (2023).

12. Abbaslou, H. Effects of mix design and curing time on compressive and tensile strength of bentonite plastic concrete. *Concrete Res.* **10** (2), 109–124 (2017).
13. Bahrami, M. & Hosseini, S. M. M. M. A new incorporative element to modify plastic concrete mechanical characteristics for cut-off wall construction in very soft soil media: identification of tensile galvanized open-mesh distributer (TGOD) element. *Constr. Build. Mater.* **350**, 128884 (2022).
14. Abbaslou, H., Ghanizadeh, A. R. & Amlashi, A. T. The compatibility of bentonite/sepiolite plastic concrete cut-off wall material. *Constr. Build. Mater.* **124**, 1165–1173 (2016).
15. Athani, S. S., Solanki, C. H. & Dodagoudar, G. R. Seepage and stability analyses of Earth dam using finite element method. *Aquat. Procedia*. **4**, 876–883 (2015).
16. Peng, M. X. & Chen, J. Slip-line solution to active Earth pressure on retaining walls. *Géotechnique* **63** (12), 1008–1019 (2013).
17. Tavana Amlashi, A., Mohammadi Golafshani, E., Ebrahimi, S. A. & Behnood, A. Estimation of the compressive strength of green concretes containing rice husk Ash: a comparison of different machine learning approaches. *Eur. J. Environ. Civil Eng.* **27** (2), 961–983 (2023).
18. Alidoust, P., Goodarzi, S., Tavana Amlashi, A. & Sadowski, Ł. Comparative analysis of soft computing techniques in predicting the compressive and tensile strength of seashell containing concrete. *Eur. J. Environ. Civil Eng.* **27** (5), 1853–1875 (2023).
19. Amlashi, A. T., Abdollahi, S. M., Goodarzi, S. & Ghanizadeh, A. R. Soft computing based formulations for slump, compressive strength, and elastic modulus of bentonite plastic concrete. *J. Clean. Prod.* **230**, 1197–1216 (2019).
20. Tavana Amlashi, A. et al. AI-based formulation for mechanical and workability properties of eco-friendly concrete made by waste foundry sand. *J. Mater. Civ. Eng.* **33** (4), 04021038 (2021).
21. Ehteram, M., Panahi, F., Ahmed, A. N., Mosavi, A. H. & El-Shafie, A. Inclusive multiple model using hybrid artificial neural networks for predicting evaporation. *Front. Environ. Sci.* **9**, 789995 (2022).
22. Albaijan, I. et al. Optimal machine learning-based method for gauging compressive strength of nanosilica-reinforced concrete. *Eng. Fract. Mech.* **291**, 109560 (2023).
23. Albaijan, I. et al. Several machine learning models to estimate the effect of an acid environment on the effective fracture toughness of normal and reinforced concrete. *Theoret. Appl. Fract. Mech.* **126**, 103999 (2023).
24. Ghanizadeh, A. R., Abbaslou, H., Amlashi, A. T. & Alidoust, P. Modeling of bentonite/sepiolite plastic concrete compressive strength using artificial neural network and support vector machine. *Front. Struct. Civil Eng.* **13**, 215–239 (2019).
25. Amlashi, A. T., Ghanizadeh, A. R., Abbaslou, H. & Alidoust, P. Developing three hybrid machine learning algorithms for predicting the mechanical properties of plastic concrete samples with different geometries. *AUT J. Civil Eng.* **4** (1), 37–54 (2020).
26. Amlashi, A. T. et al. Application of computational intelligence and statistical approaches for auto-estimating the compressive strength of plastic concrete. *Eur. J. Environ. Civil Eng.* **26** (8), 3459–3490 (2022).
27. Alishvandi, A. et al. *Estimating the Compressive Strength of Plastic Concrete Samples Using Machine Learning Algorithms* (Asian Journal of Civil Engineering, 2023).
28. Zhou, Z. H. *Ensemble Methods: Foundations and Algorithms* (CRC, 2012).
29. Li, Q. F. & Song, Z. M. High-performance concrete strength prediction based on ensemble learning. *Constr. Build. Mater.* **324**, 126694 (2022).
30. Feng, D. C. et al. Machine learning-based compressive strength prediction for concrete: an adaptive boosting approach. *Constr. Build. Mater.* **230**, 117000 (2020).
31. Ekanayake, I., Meddage, D. & Rathnayake, U. A novel approach to explain the black-box nature of machine learning in compressive strength predictions of concrete using Shapley additive explanations (SHAP). *Case Stud. Constr. Mater.*, **16**, e01059. (2022).
32. Lv, Y., Shi, X., Ran, L. & Shang, M. Random forest-based ensemble estimator for concrete compressive strength prediction via adaboost method. In Advances in Natural Computation, Fuzzy Systems and Knowledge Discovery: Volume 2 (557–565). Springer International Publishing. (2020).
33. Xu, Y. et al. Computation of high-performance concrete compressive strength using standalone and ensembled machine learning techniques. *Materials* **14** (22), 7034 (2021).
34. Rathakrishnan, V., Beddu, S., Bt & Ahmed, A. N. Predicting compressive strength of high-performance concrete with high volume ground granulated blast-furnace slag replacement using boosting machine learning algorithms. *Sci. Rep.* **12** (1), 9539 (2022).
35. Nisar, N. & Bhat, J. A. Experimental investigation of rice husk Ash on compressive strength, carbonation and corrosion resistance of reinforced concrete. *Australian J. Civil Eng.* **19** (2), 155–163 (2021).
36. Zeng, Z. et al. Accurate prediction of concrete compressive strength based on explainable features using deep learning. *Constr. Build. Mater.* **329**, 127082 (2022).
37. Shang, M. et al. Predicting the mechanical properties of RCA-based concrete using supervised machine learning algorithms. *Materials* **15** (2), 647 (2022).
38. Pan, X. et al. Use of artificial intelligence methods for predicting the strength of recycled aggregate concrete and the influence of Raw ingredients. *Materials* **15** (12), 4194 (2022).
39. Amin, M. N. et al. Split tensile strength prediction of recycled aggregate-based sustainable concrete using artificial intelligence methods. *Materials* **15** (12), 4296 (2022).
40. Ullah, H. S. et al. Prediction of compressive strength of sustainable foam concrete using individual and ensemble machine learning approaches. *Materials* **15** (9), 3166 (2022).
41. Amin, M. N. et al. Prediction of mechanical properties of Fly-Ash/Slag-Based geopolymer concrete using ensemble and Non-Ensemble Machine-Learning techniques. *Materials* **15** (10), 3478 (2022).
42. Ahmad, A. et al. Prediction of geopolymer concrete compressive strength using novel machine learning algorithms. *Polymers* **13** (19), 3389 (2021).
43. Hoang, N. D. Machine Learning-Based Estimation of the compressive strength of Self-Compacting concrete: A Multi-Dataset study. *Mathematics* **10** (20), 3771 (2022).
44. Nafees, A. et al. Forecasting the mechanical properties of plastic concrete employing experimental data using machine learning algorithms: DT, MLPNN, SVM, and RF. *Polymers* **14** (8), 1583 (2022).
45. Amin, M. N. et al. Prediction model for rice husk Ash concrete using AI approach: boosting and bagging algorithms. In Structures (Vol. 50, 745–757). Elsevier. (2023).
46. Li, Q. & Song, Z. Prediction of compressive strength of rice husk Ash concrete based on stacking ensemble learning model. *J. Clean. Prod.* **382**, 135279 (2023).
47. Iftikhar, B. et al. Predictive modeling of compressive strength of sustainable rice husk Ash concrete: ensemble learner optimization and comparison. *J. Clean. Prod.* **348**, 131285 (2022).
48. Qu, Z. et al. A combined genetic optimization with adaboost ensemble model for anomaly detection in buildings electricity consumption. *Energy Build.* **248**, 111193 (2021).
49. Long, J. S. & Freese, J. Regression models for categorical dependent variables using Stata (Vol. 7). Stata press. (2006).
50. McCaffrey, D. F., Ridgeway, G. & Morral, A. R. Propensity score Estimation with boosted regression for evaluating causal effects in observational studies. *Psychol. Methods*. **9** (4), 403 (2004).
51. Claesen, M. & De Moor, B. Hyperparameter search in machine learning. arXiv preprint arXiv:1502.02127. (2015).
52. Feurer, M. & Hutter, F. Hyperparameter optimization. In Automated Machine Learning: Methods, Systems, Challenges (pp. 3–33). (2019).

53. Yang, L. & Shami, A. On hyperparameter optimization of machine learning algorithms: theory and practice. *Neurocomputing* **415**, 295–316 (2020).
54. Tayebi, M., Kafhali, E. & S *Performance Analysis of Metaheuristics Based Hyperparameters Optimization for Fraud Transactions Detection* (Evolutionary Intelligence, 2022).
55. Duan, J., Asteris, P. G., Nguyen, H., Bui, X. N. & Moayedi, H. A novel artificial intelligence technique to predict compressive strength of recycled aggregate concrete using ICA-XGBoost model. *Eng. Comput.* **37**, 3329–3346 (2021).
56. Alhakeem, Z. M. et al. Prediction of ecofriendly concrete compressive strength using gradient boosting regression tree combined with GridSearchCV hyperparameter-optimization techniques. *Materials* **15** (21), 7432 (2022).
57. Yang, H., Liu, X. & Song, K. A novel gradient boosting regression tree technique optimized by improved sparrow search algorithm for predicting TBM penetration rate. *Arab. J. Geosci.* **15** (6), 461 (2022).
58. Moradi Moghaddam, H. et al. Shear modulus prediction of landfill components using novel machine learners hybridized with forensic-based investigation optimization. *Constr. Build. Mater.* **411**, 134443 (2024).
59. Schapire, R. E. The strength of weak learnability. *Mach. Learn.* **5**, 197–227 (1990).
60. Freund, Y., Schapire, R. & Abe, N. A short introduction to boosting. *Journal-Japanese Soc. Artif. Intell.* **14**, 1612 (1999).
61. Ying, C., Qi-Guang, M., Jia-Chen, L. & Lin, G. Advance and prospects of adaboost algorithm. *Acta Automatica Sinica*. **39** (6), 745–758 (2013).
62. Safavian, S. R. & Landgrebe, D. A survey of decision tree classifier methodology. *IEEE Trans. Syst. Man. Cybernetics*. **21** (3), 660–674 (1991).
63. Breiman, L. *Classification and Regression Trees* (Routledge, 2017).
64. Prasad, A. M., Iverson, L. R. & Liaw, A. Newer classification and regression tree techniques: bagging and random forests for ecological prediction. *Ecosystems* **9**, 181–199 (2006).
65. Ding, C., Wu, X., Yu, G. & Wang, Y. A gradient boosting logit model to investigate Driver's stop-or-run behavior at signalized intersections using high-resolution traffic data. *Transp. Res. Part. C: Emerg. Technol.* **72**, 225–238 (2016).
66. Li, H., Sun, J. & Wu, J. Predicting business failure using classification and regression tree: an empirical comparison with popular classical statistical methods and top classification mining methods. *Expert Syst. Appl.* **37** (8), 5895–5904 (2010).
67. He, Q., Kamarianakis, Y., Jintanakul, K. & Wynter, L. Incident duration prediction with hybrid tree-based quantile regression. In Advances in Dynamic Network Modeling in Complex Transportation Systems (pp. 287–305). (2013).
68. Bevilacqua, M., Braglia, M. & Montanari, R. The classification and regression tree approach to pump failure rate analysis. *Reliab. Eng. Syst. Saf.* **79** (1), 59–67 (2003).
69. Chen, T. et al. Xgboost: extreme gradient boosting. *R Package Version 0 4-2*. **1 (4)**, 1–4 (2015).
70. Svetnik, V. et al. Random forest: a classification and regression tool for compound classification and QSAR modeling. *J. Chem. Inf. Comput. Sci.* **43** (6), 1947–1958 (2003).
71. Zhang, J., Ma, G., Huang, Y., Aslani, F. & Nener, B. Modelling uniaxial compressive strength of lightweight self-compacting concrete using random forest regression. *Constr. Build. Mater.* **210**, 713–719 (2019).
72. Zhang, J., Wang, R., Lu, Y. & Huang, J. Prediction of compressive strength of geopolymer concrete landscape design: application of the novel hybrid RF–GWO–XGBoost algorithm. *Buildings* **14** (3), 591 (2024).
73. Ly, H. B., Nguyen, M. H. & Pham, B. T. Metaheuristic optimization of Levenberg–Marquardt-based artificial neural network using particle swarm optimization for prediction of foamed concrete compressive strength. *Neural Comput. Appl.* **33** (24), 17331–17351 (2021).
74. Bui, D. T., Abdullahi, M. A. M., Ghareh, S., Moayedi, H. & Nguyen, H. Fine-tuning of neural computing using Whale optimization algorithm for predicting compressive strength of concrete. *Eng. Comput.* **37**, 701–712 (2021).
75. Moghaddam, H. M., Fahimifar, A., Ebadi, T., Keramati, M. & Siddiqua, S. *Assessment of leachate-contaminated Clays Using Experimental and Artificial Methods* (Journal of Rock Mechanics and Geotechnical Engineering, 2024).
76. Chou, J. S. & Nguyen, N. M. FBI inspired meta-optimization. *Appl. Soft Comput.* **93**, 106339 (2020).
77. Hu, L. M., Gao, D. Y., Li, Y. Z. & Song, S. Q. Analysis of the influence of long curing age on the compressive strength of plastic concrete. *Adv. Mater. Res.* **38**, 200–203 (2012).
78. Pisheh, Y. P. & Hosseini, S. M. M. Stress-strain behavior of plastic concrete using monotonic triaxial compression tests. *J. Cent. South. Univ.* **19** (4), 1125–1131 (2012).
79. Tahershamsi, A., Bakhtiyari, A. & Binazadeh, N. Effects of clay mineral type and content on compressive strength of plastic concrete (In Persian). *Iran. J. Min. Eng.* **4** (7), 35–42 (2009).
80. Guan, Q. Y. & Zhang, P. *Effect of Clay Dosage on Mechanical Properties of Plastic Concrete* (in Advanced Materials Research, Trans Tech Publ, 2011).
81. Zhang, P. & Guan, Q. Y. Mechanical properties of plastic concrete containing bentonite. *Res. J. Appl. Sci. Eng. Technol.* **5** (4), 1317–1322 (2013).
82. Mousavi, S. M., Aminian, P., Gandomi, A. H., Alavi, A. H. & Bolandi, H. A new predictive model for compressive strength of HPC using gene expression programming. *Adv. Eng. Softw.* **45** (1), 105–114 (2012).
83. Mahboubi, A. & Ajorloo, A. Experimental study of the mechanical behavior of plastic concrete in triaxial compression. *Cem. Concr. Res.* **35** (2), 412–419 (2005).
84. Pashazadeh, A. & Chekani Azar, M. Estimating an appropriate plastic concrete mixing design for Cut-off walls to control leakage under the Earth dam. *J. Basic Appl. Sci. Res.* **1** (9), 1295–1299 (2011).
85. Elwell, D. J. & Fu, G. Compression testing of concrete: cylinders vs. cubes. (1995).
86. Iqbal, M. F. et al. Prediction of mechanical properties of green concrete incorporating waste foundry sand based on gene expression programming. *J. Hazard. Mater.* **384**, 121322 (2020).
87. Asteris, P. G., Ashrafian, A. & Rezaie-Balf, M. Prediction of the compressive strength of self-compacting concrete using surrogate models. *Comput. Concr.* **24** (2), 137–150 (2019).
88. Golafshani, E. M. & Behnood, A. Predicting the mechanical properties of sustainable concrete containing waste foundry sand using multi-objective ANN approach. *Constr. Build. Mater.* **291**, 123314 (2021).
89. Ashrafian, A., Gandomi, A. H., Rezaie-Balf, M. & Emadi, M. An evolutionary approach to formulate the compressive strength of roller compacted concrete pavement. *Measurement* **152**, 107309 (2020).
90. Lundberg, S. M. & Lee, S. I. A unified approach to interpreting model predictions. *Adv. Neural. Inf. Process. Syst.*, 30. (2017).
91. Heidarabadizadeh, N., Ghanizadeh, A. R. & Behnood, A. Prediction of the resilient modulus of non-cohesive subgrade soils and unbound subbase materials using a hybrid support vector machine method and colliding bodies optimization algorithm. *Constr. Build. Mater.* **275**, 122140 (2021).
92. Golafshani, E. M. & Behnood, A. Estimating the optimal mix design of silica fume concrete using biogeography-based programming. *Cem. Concr. Compos.* **96**, 95–105 (2019).
93. Golafshani, E. M. & Behnood, A. Application of soft computing methods for predicting the elastic modulus of recycled aggregate concrete. *J. Clean. Prod.* **176**, 1163–1176 (2018).
94. Chou, J. S., Chen, L. Y. & Liu, C. Y. Forensic-based investigation-optimized extreme gradient boosting system for predicting compressive strength of ready-mixed concrete. *J. Comput. Des. Eng.* **10** (1), 425–445 (2023).
95. BPC-EL online application. (2024). https://colab.research.google.com/drive/1a3pjScLsripH-756yYk2nyol5g7HM9U1

Acknowledgements
The authors would like to convey their appreciation to all individuals who contributed to the study. We sincerely thank Dr. Samer Dessouky and Dr. Alireza Ghanizadeh for their invaluable guidance and support throughout this research. Also, we express our gratitude to the participants and facilities that facilitated the settings for our experiments and data collecting, assuring our field investigations' triumph.

Author contributions
Amir Tavana Amlashi, Haytham F. Isleem, Mohammad Khishe: Conceptualization, Investigation, Resources, Writing-Original draft. Project administration Ali Reza Ghanizadeh, Haytham F. Isleem, Mohammad Khishe: Methodology, Validation, Software, Visualization, Supervision. Shadi Firouzranjbar: Investigation, Hossein Moradi Moghaddam: Writing-Original draft. Mohsen Navazani: Software, Visualization. Samer Dessouky: Supervision, Writing - Review and Editing.

Funding information verification
This research received no specific grant from funding agencies in the public, commercial, or not-for-profit sectors.

Declarations

Competing interests
The authors declare no competing interests.

Additional information
Correspondence and requests for materials should be addressed to A.T.A., H.F.I. or M.K.

Reprints and permissions information is available at www.nature.com/reprints.

Publisher's note Springer Nature remains neutral with regard to jurisdictional claims in published maps and institutional affiliations.